AGU ADVANCING EARTH AND SPACE SCIENCE

JGR Oceans

Key Points:

- Measurements from diverse oceanic environments are used to characterize variability in the size distribution of suspended particles
- A power law model performs poorly in estimating relative contributions of three size classes to the particle size distribution
- A novel approach is developed that utilizes percentiles of the cumulative particle size distribution to predict size class contributions

Correspondence to:

R. A. Reynolds,
rreynolds@ucsd.edu

Variability in Oceanic Particle Size Distributions and Estimation of Size Class Contributions Using a Non-parametric Approach

Rick A. Reynolds[1] [ID] and Dariusz Stramski[1] [ID]

[1]Marine Physical Laboratory, Scripps Institution of Oceanography, University of California San Diego, La Jolla, CA, USA

Abstract A dataset of nearly 400 measurements of the particle size distribution (PSD) compiled from the Pacific, Atlantic, and Arctic Oceans is used to examine variability in the magnitude and shape of the PSD, and to characterize the partitioning of particle number, cross-sectional area, and volume concentration among defined size intervals. The results indicate that the relative contributions of three size classes based upon the pico-, nano-, and microplankton size range exhibit substantial changes among measures of particle size and between oceanic environments. The single-slope power law model commonly employed to characterize the PSD in aquatic studies is demonstrated to have significant limitations in capturing the complexity of PSD shapes observed for natural particle assemblages, and in consequence poorly predicts the relative contributions of these different size intervals. We show that specific percentile diameters derived from the cumulative distributions of particle size are strongly correlated with the contributions of these three size classes, and that these non-parametric descriptors of the cumulative distribution provide superior performance for estimating their contributions while requiring no assumption of underlying PSD shape. A comparison of these predictive relationships with independent field measurements suggests that this approach is generally robust for particle assemblages representing a wide diversity of marine environments.

Plain Language Summary The particle size distribution (PSD) describes how the concentration of particles changes with particle size, and it is an important characteristic of suspended oceanic particles that influences ocean ecology and biogeochemistry. We analyze an extensive set of measurements of the PSD from the Pacific, Atlantic, and Arctic Oceans to characterize how different size classes of particles contribute to the total concentration of particle number, cross-sectional area, and volume. Our results quantify this partitioning and demonstrate the variability observed among different oceanic environments. A frequently used model of the PSD employed for aquatic studies is shown to have strong limitations in representing these measurements of natural samples, and consequently performs poorly in estimating the relative contributions of individual size classes. We show that a novel approach of describing the PSD based on specific percentile diameters derived from the cumulative distribution of size-dependent particle concentration provides a better means to characterize the shape of the PSD for oceanic particle assemblages, and provides superior performance in estimating size class contributions in diverse marine environments. Further research establishing relationships between these percentile diameters and optical proxies obtained from autonomous sensing platforms could greatly extend the observational capabilities of particle size in the oceanic environment.

1. Introduction

Particles suspended in seawater play an important role in regulating marine biogeochemical cycles, ecological processes, and the sequestering of carbon from the atmosphere to the deep ocean. As many particle-mediated processes are dependent upon the size of the particle, knowledge of the particle size distribution (PSD) is required for understanding numerous physical, chemical, and biological processes within the ocean. For example, the PSD strongly influences the absorption, scattering, and penetration of light through the water column (Baker & Lavelle, 1984; Morel & Bricaud, 1986), planktonic growth and metabolic processes (Chisholm, 1992; Marañón, 2015), trophic interactions (Jennings & Warr, 2003; Le Quéré et al., 2005; Parsons, 1969; Ward et al., 2012), particle aggregation and dissolution (Burd, 2013; Jackson, 1995), and gravitational sinking of particulate material to depth (Stemmann et al., 2004).

The PSD describes the average concentration of particles within discrete size intervals for a given volume of suspension. Particle concentration may be defined in multiple ways (e.g., particle number, area, volume, or mass

concentration) depending upon measurement technique or the scientific question of interest, and these different measures can be interconverted through assumptions of particle shape or density. The function describing the particle numerical concentration per unit size interval as a function of particle diameter D, $N'(D)$ [m^{-3} μm^{-1}], is one basic description of the relationship between particle abundance and size. Integration of this continuous function over a defined size interval yields the total number of particles per unit volume, $N(D)$ [m^{-3}], associated with the given size range. The use of a single metric to characterize particle size has inherent limitations when applied to natural assemblages of oceanic particles, which are comprised of heterogeneous mixtures of particles exhibiting diverse and complex three-dimensional shapes. An additional complication is that different particle-sizing methods provide different measures of particle size depending on the underlying measurement principle (Jonasz & Fournier, 2007). In the present study, the particle diameter D represents the diameter of a volume-equivalent spherical particle but must be recognized as only one means to approximate the true particle "size".

In marine environments, the PSD is continually varying in time and space as natural processes alter both the concentrations and sizes of particles within a given volume of seawater. Despite increasing capabilities to measure the PSD in oceanic waters (Agrawal & Pottsmith, 2000; Graham & Nimmo-Smith, 2010; Jackson et al., 1997; Moore et al., 2009; Picheral et al., 2010), in situ measurements alone cannot provide the spatial or temporal resolution needed to characterize global oceanic ecosystems. For this reason, efforts to develop remote-sensing approaches for estimation of the PSD from airborne or satellite measurements of ocean color have been pursued (Bowers et al., 2007; Kostadinov et al., 2009, 2010; Lei et al., 2021; Shi & Wang, 2019). These approaches generally rely on empirical parameterizations or simplified descriptions of the PSD in order to quantify relationships between the PSD and the optical properties of seawater.

Several formulations for describing and modeling the size distribution of marine particles have been proposed and utilized in past studies (e.g., Bader, 1970; Barndorff-Nielsen, 1977; Jonasz & Fournier, 2007; Kranck & Milligan, 1992; Lambert et al., 1981; Risović, 1993; Zhang et al., 2012). These analytical descriptions of the PSD are well suited to numerical modeling, facilitate the calculation of various statistical metrics derived from the distribution, and allow easy quantification of the relative contributions of different size ranges. The power law function, first used by Bader (1970) to describe marine particle size distributions, is the most commonly used parameterization. It is often referred to as the Junge function, who used it to describe the size distribution of atmospheric aerosols (Junge, 1963). The density function of particle number concentration for this model can be written as

$$N'(D) = N'_o \left(D/D_o \right)^{\zeta_N} \tag{1}$$

where D_o is a reference diameter [μm], N'_o [m^{-3} μm^{-1}] is the value of N' at D_o, and ζ_N is the dimensionless slope of the distribution which is assumed constant throughout the entire size range. In aquatic ecosystems, the particle number concentration over a large size range invariably decreases with increasing particle size and thus the exponent ζ_N is negative. A number of biological arguments have been advanced to justify the use of this function based on considerations of ecological structure and predator-prey relationships in planktonic ecosystems (e.g., Kiefer & Berwald, 1992; Platt & Denman, 1978; Rinaldo et al., 2002; Sheldon et al., 1977).

The power law model remains in widespread use and can provide a reasonable approximation of the PSD over limited size ranges in some environments (e.g., Buonassissi & Dierssen, 2010; Reynolds et al., 2010). However, as noted by Bader (1970) himself, the PSD measured in natural waters often exhibits "irregularities" which challenge the use of a single slope over a broad range of particle sizes. Field studies have highlighted such limitations when applying the model to describe natural oceanic particle assemblages. In oceanic or coastal waters rich in plankton the PSD frequently exhibits distinct peaks and valleys reflecting growth or removal of microbial species within distinct size classes (Jonasz, 1983; Organelli et al., 2020; Reynolds et al., 2010; Sheldon et al., 1972). For waters in which the particles are predominantly non-living, the PSD may be relatively featureless but can exhibit significant changes in slope for different portions of the size range (Bochdansky et al., 2016; Reynolds et al., 2016; Stavn, 2004; Woźniak et al., 2010). Such observations have led to proposed modifications of the power law model that include the use of multiple slope parameters for different size ranges (Gordon & Brown, 1972; Qiu et al., 2016), or varying slope as a function of size (Ceronio & Haarhoff, 2005; Lawler, 1997). Alternative formulations of the PSD have also met with mixed success, proving adequate in some environments but perform-

ing poorly in others. These observations are unsurprising as it is unlikely that a single universal function describing the shape of the PSD can adequately capture all scenarios possible in natural waters.

For many investigations, the detailed shape of the PSD is not needed and a coarser description of the relative concentrations of different particle size classes provides sufficient information on particle size. Models to describe particle transport and dynamics, for example, frequently distinguish between single grain (fine) and various aggregate (flocs) particles which are generally defined according to a size range (e.g., Kranck & Milligan, 1992; Mikkelsen et al., 2006). In plankton ecology, the size structure of the plankton community is often described by the relative abundance of defined size classes which exhibit different biogeochemical and ecological roles (Sieburth et al., 1978). Phytoplankton, for example, are commonly classified by assigning taxa to one of three size classes referred to as pico- ($D < 2$ μm), nano- ($D = 2$–20 μm) and microphytoplankton ($D > 20$ μm) (IOC-CG, 2014). Such simplifications have the benefit of distilling the complex nature of the oceanic PSD into a few metrics that can be used to address scientific questions.

In a recent study based on the analysis of 168 measurements collected in waters of the western Arctic Ocean, we described variability in the shape and relative contributions of different size classes for distributions of particle size based on the number, cross-sectional area, and volume concentration (Runyan et al., 2020). We also demonstrated that specific percentile diameters derived from the cumulative distribution of particle size were well-correlated with the relative contributions of the pico-, nano-, and microplankton size classes, and provided superior performance in predicting these contributions compared to a single-slope power law model. A major advantage in the use of these non-parametric descriptors is that no a priori assumption regarding the PSD shape is needed, and thus this approach can accommodate the generally complex shapes that are frequently observed in the particle size distributions of natural seawater samples. In this study we extend this analysis by the addition of a new field dataset of 226 PSD measurements collected in lower latitude regions of the Pacific and Atlantic Oceans. We examine the shape of the PSD and the relative partitioning of size among three size classes in these environments, and investigate relationships between various percentile diameters of the cumulative distribution and the fractional contributions of these planktonic intervals to particle concentration. Using this combined dataset of 394 field observations from the Arctic, Pacific, and Atlantic Oceans, we develop models to estimate the relative contributions of the pico-, nano-, and microplanktonic size classes. These models are then evaluated with an independent dataset from the Atlantic Ocean. Our results support the conclusion that percentile-based models provide much better performance than the power law model to estimate these size class contributions, and suggest that this approach is applicable to a wide variety of marine environments.

2. Materials and Methods

2.1. Study Areas and Sampling

In this study we introduce a new dataset, referred to as PacAtl, that is comprised of 226 field measurements of the PSD compiled from five cruises in the Pacific and Atlantic Oceans (Table 1). The observations span different oceanic regions (Figure 1), with surface concentrations of chlorophyll-*a* (Chla) ranging from 0.02 mg m^{-3} in the ultra-oligotrophic South Pacific Subtropical Gyre to maximal values of 1.5 mg m^{-3} observed in the North Atlantic off the western coast of Brittany. Corresponding surface values of particulate organic carbon concentration (POC) in this dataset exhibit a similar broad range from 12 to 258 mg m^{-3}.

Sampling in the Atlantic Ocean was conducted along a transect from Chile to Germany between April 7 and May 17, 2010 as part of the ANTXXVI/4 cruise on the R/V Polarstern (Uitz et al., 2015). Field observations in the Pacific Ocean were obtained on four different cruises. The BIOSOPE (BIogeochemistry and Optics SOuth Pacific Experiment) expedition on the R/V L'Atalante sampled waters along a west-to-east transect in the eastern South Pacific Ocean between the Marquesas Islands and the coast of Chile from October 17 to December 15, 2004 (Claustre et al., 2008). Only observations from Leg 1 of this cruise between the Marquesas Islands and Easter Island are utilized here. Data from two cruises on the R/V Kilo Moana as part of the Radiance in a Dynamic Ocean (RaDyO) program (Dickey et al., 2012; Stramski et al., 2019) sampled mesotrophic waters in the Santa Barbara (SB) Channel (KM08-18; 3–25 September 2008) and tropical waters off the coast of the Hawaiian Islands (KM09-21; August 24 to September 15, 2009). A third cruise on the Kilo Moana (KM12-10; May 28 to June 10, 2012) also sampled Hawaiian waters as part of an ONR-sponsored MURI project (Johnsen et al., 2014).

Table 1
Description of the Field Datasets of PSD Measurements Used in This Study

Cruise	Region	PSD measurement	Size range	Total (n)	Surface (n)	z_{max} (m)
PacAtl (n = 226)						
ANTXXVI/4	Atlantic	Coulter 30 & 200 μm aperture	0.7–120 μm	43	22	140
BIOSOPE	S. Pacific	Coulter 30 μm aperture & HIAC	0.6–100 μm	146	62	504
KM08-18	SB Channel	Coulter 30 & 200 μm aperture	0.8–120 μm	17	12	122
KM09-21	Hawaii	Coulter 30 & 200 μm aperture	0.7–120 μm	14	8	150
KM12-10	Hawaii	Coulter 30 & 200 μm aperture	0.7–120 μm	6	5	130
Arctic (n = 168)						
MALINA	Arctic	Coulter 30 & 200 μm aperture	0.7–120 μm	40	18	80
HLY1001	Arctic	Coulter 30 & 200 μm aperture	0.7–120 μm	30	24	46
HLY1101	Arctic	Coulter 30 & 200 μm aperture	0.7–120 μm	53	24	300
MR17-05C	Arctic	Coulter 30 & 200 μm aperture	0.7–120 μm	45	20	125

Note. In addition to the total number n of PSD measurements obtained on each cruise, the number of samples from the near surface layer and the maximum sample depth (z_{max}) are also provided.

Abbreviation: SB, Santa Barbara.

On all cruises, discrete water samples were obtained from one or more depths at each station using a CTD-Rosette equipped with Niskin bottles. The near surface layer (nominally 1–5 m depth) was sampled at every station and consequently surface data comprise nearly half of the PacAtl measurements, with the maximum depth of sampling varying among individual cruises (Table 1). For most stations, additional samples were obtained at depths corresponding to features within the upper water column such as maxima in chlorophyll-*a* fluorescence or the optical beam attenuation coefficient, or from depths below the surface mixed layer. All PSD measurements were made onboard the research vessels and began immediately following sample collection.

In addition to these data, we also incorporate for our analyses an additional 168 measurements of the PSD obtained from four cruises in western Arctic waters (Figure 1, Table 1). A detailed description of these cruises and sampling methodology are available in Runyan et al. (2020). Briefly, the MALINA (MAckenzie LIght aNd cARbon) cruise sampled the southeastern Beaufort Sea from July 31 to August 24, 2009 on the CCGS Amundsen. Two cruises of the NASA ICESCAPE (Impacts of Climate on EcoSystems and Chemistry of the Arctic Pacific Environment) program utilized the USCGC Healy to sample the Chukchi Sea and western Beaufort Sea during two successive years; the HLY1001 cruise from June 18 through July 16, 2010 and the HLY1101 cruise from June 28 through July 24, 2011. The MR1705-C cruise took place onboard the R/V Mirai from August 26 to September 18, 2017 as part of the Japanese ArCS (Arctic Challenge for Sustainability) program, with sampling conducted from the Bering Strait to the southern limit of the ice edge at about 76.5°N. A notable feature of the data from these four cruises is a very broad range observed in surface concentrations of both Chla (0.02–29 mg m^{-3}) and POC (15–1022 mg m^{-3}).

Similar to the PacAtl dataset, near surface measurements (1–5 m depth) comprise the majority of the Arctic dataset with additional measurements obtained at depths corresponding to observed features or from below the mixed layer. For stations located on the continental shelf, samples were also obtained from depths within 3–5 m of the sea bottom. Importantly, however, all measurements of particle size on these Arctic cruises were obtained in an identical manner to most of the PacAtl dataset.

2.2. Measurements of the Particle Size Distribution

Particle size distribution measurements were obtained on all cruises with a Beckman-Coulter Multisizer III. The measurement principle utilizes changes
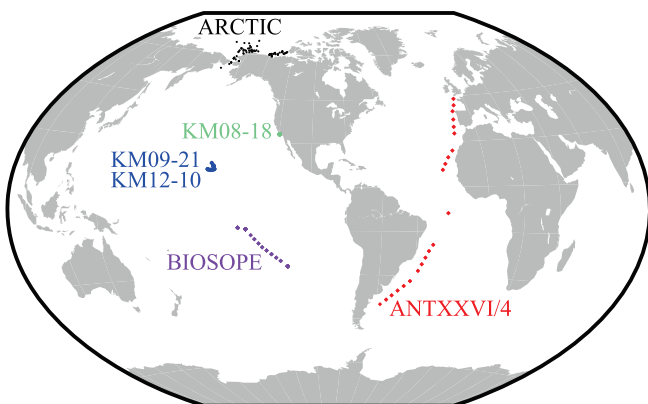

Figure 1. Sampling locations of particle size distribution (PSD) measurements for the cruises described in Table 1.

in the electrical impedance of a diluent to count and size particles as they pass through an aperture of known size, and has long been used in the study of oceanic particle size distributions (Brun-Cottan, 1971; Carder et al., 1971; Jackson et al., 1997; Jonasz, 1983; Kitchen et al., 1975; Parsons, 1969; Sheldon et al., 1972). Multiple studies have intercompared PSD measurements obtained using a Coulter counter with other particle-sizing instrumentation (Jonasz & Fournier, 2007), including intercomparisons involving natural assemblages of marine particles (Reynolds et al., 2010, 2016). Despite the inherent challenges in comparing results between instruments that utilize different operating principles and methods of defining particle size, such studies have generally indicated moderate to good agreement between results obtained by the Coulter counter with other techniques.

For all cruises except BIOSOPE, water samples were measured with a combination of 30 and 200 µm aperture sizes and the results merged to yield particle concentrations over the nominal size range $D = 0.6$–120 µm, where D represents the volume-equivalent spherical diameter. Filtered (0.2 µm) seawater was used as the diluent and blank, and both apertures were calibrated using suspensions of NIST-traceable microsphere standards of known size.

Typical interrogated volumes for a single measurement ranged from 0.1 to 0.5 cm³ for the 30 µm aperture and from 2 to 18 cm³ for the 200 µm aperture. For each seawater sample, multiple (generally >25) replicate measurements of the PSD were acquired for each aperture size and summed together to increase sampling volume and counting accuracy. For the combined PacAtl and Arctic datasets, the average cumulative sample volume of each Coulter PSD measurement was 2.5 ± 1.5 cm³ (number of observations $n = 394$; mean $\pm$ standard deviation) for the 30 µm aperture and 189 ± 84 cm³ ($n = 248$) for the 200 µm aperture. Volumes higher than these average values were generally associated with measurements in the clearest waters (e.g., BIOSOPE and KM cruises in Hawaii), and smaller volumes were obtained in more turbid waters (e.g., Arctic cruises).

Each measurement with a given aperture provided the number of particles per unit volume, N [m⁻³], for 256 or 300 discrete size bins of logarithmically-increasing bin width. The nominal measurement size range is 2%–60% of the aperture diameter, corresponding to 0.6–18 µm for the 30 µm aperture and 4–120 µm for the 200 µm aperture. The density function of the number concentration as a function of diameter, $N'(D)$ [m⁻³ µm⁻¹], was calculated by dividing the measured concentration of particles within each size bin by the bin width. To create the final distribution, measurements of $N'(D)$ from both apertures were merged at an overlapping size bin which shared a similar midpoint and bin width. This merging was performed at $D = 4.8 \pm 0.03$ µm for all cruises except for KM08-18, where the merging was done at 5.11 ± 0.03 µm. The magnitude of $N'(D)$ at this overlapping size bin was scaled to the same value for both apertures, and the resulting merged distribution was converted back to $N(D)$ through multiplication of $N'(D)$ for each bin by the bin width.

For the BIOSOPE expedition, only measurements with the 30 µm aperture were obtained routinely. To achieve PSDs for a size range similar to the other cruises, we combined results from the Coulter 30 µm aperture with concomitant onboard measurements obtained with a HIAC/Royco 3001 particle counter (Pacific Scientific). The HIAC is an optical based counter which measures the attenuation of a laser beam to detect and size particles as they pass through a glass microcell. The amplitude of detected pulses is assumed to be proportional to particle size, and similar to the Coulter is calibrated with microspheres of known size and refractive index. Additional information on the HIAC methods employed on the BIOSOPE cruise are available in Stemmann et al. (2008).

The HIAC provided measurements of particle concentration in 50 size bins of logarithmically-increasing width over the size range $D = 1.5$–100 µm. To merge these results with the Coulter data, seven Coulter 30 µm aperture bins were aggregated to create a combined bin of size $D = 5.21 \pm 0.21$ µm that closely matched a HIAC bin in this size range. The particle concentration estimates between Coulter and HIAC in this matched size bin generally exhibited reasonable agreement (average difference of 27.5%), as previously noted by Stemmann et al. (2008). The two size distributions were then combined in a similar fashion as described previously for the merging of the Coulter 30 and 200 µm apertures. The final Coulter/HIAC merged distributions span the size range $D = 0.6$–100 µm.

All merged size distributions up to $D = 30$ µm were smoothed twice with a 3- or 5-bin moving average (depending on size range) to reduce small bin-to-bin variations in measured particle concentrations. Low particle counts were frequently observed for $D > 30$ µm, thus the measured PSDs in this size range were rebinned by aggregating 3 to 40 individual bins to create larger size intervals with increased particle counts. This rebinning was also performed for the BIOSOPE merged size distributions where HIAC data was used in lieu of Coulter 200 µm aperture

measurements, and has the additional benefit of yielding bin sizes in this size range comparable to the other PSDs measured with the Coulter.

On some cruises, the lower nominal limit of $D = 0.6$ μm for the 30 μm aperture could not routinely be achieved owing to elevated instrument noise levels. For the analyses presented in this study, all distributions have been truncated to a lower limit of $D = 0.8$ μm to ensure consistency in the measured size range among all cruises and to avoid regions of potentially high instrument noise. These final distributions consist of 302 size bins spanning the range of D from 0.8 to 120 μm, with bin widths varying from 0.01 to 52 μm. The BIOSOPE data of combined Coulter and HIAC PSDs comprise 191 bins over the range D from 0.8 to 100 μm with widths varying from 0.01 to 35 μm. Detailed information on the final individual size bins for each PSD used in this study data are available on the Dryad repository (Reynolds & Stramski, 2021).

2.3. Analysis of Measured Particle Size Distributions

The concentrations of particle cross-sectional area, $A(D)$ [m^2 m^{-3}], and particle volume, $V(D)$ [m^3 m^{-3}], within each size bin were calculated from the final merged $N(D)$ by assuming spherical particles and the relations $A(D) = N(D) \pi D^2/4$ and $V(D) = N(D) \pi D^3/6$. Corresponding density functions for the concentrations of particle area, $A'(D)$ [m^2 m^{-3} μm^{-1}], and particle volume, $V'(D)$ [m^3 m^{-3} μm^{-1}], were then computed in a manner analogous to that of $N'(D)$ by dividing each value of $A(D)$ and $V(D)$ by the bin width.

To characterize the PSDs, cumulative distributions for the concentrations of particle number, $C_N(D)$, cross-sectional area, $C_A(D)$, and volume, $C_V(D)$, were calculated from the respective density functions, $N'(D)$, $A'(D)$, and $V'(D)$. For example, in the case of the particle number concentration the cumulative distribution $C_N(D)$ was computed according to

$$C_N(D) = \int_{0.8}^{D} N'(D) \, dD \Big/ \int_{0.8}^{D\max} N'(D) \, dD \tag{2}$$

where the integration limits represent D in μm. The value of $D_{\max}$ was 120 μm in all cases except for BIOSOPE where $D_{\max}$ is equal to 100 μm. The cumulative distributions $C_A(D)$ and $C_V(D)$ were calculated in a similar manner by replacing $N'(D)$ in Equation 2 with $A'(D)$ and $V'(D)$, respectively. The particle diameters corresponding to discrete percentiles of the cumulative distribution functions for particle number, area, and volume concentrations were then determined for each sample. The integral in the denominator of Equation 2 is equivalent to the total particle number concentration over the measured size range, N_t [m^{-3}]. Similarly, the total concentrations of particle area, A_t [μm^2 m^{-3}], and volume, V_t [μm^3 m^{-3}], were calculated using the denominator of Equation 2 and replacing $N'(D)$ with $A'(D)$ and $V'(D)$, respectively.

Additional metrics to characterize the relative shapes of the PSDs were calculated by quantifying the fractional contributions f of discrete size ranges to the values of N_t, A_t, and V_t. In this study, we chose three discrete size ranges to approximate the plankton size classification scheme of Sieburth et al. (1978); picoplankton (f_{pico}; $0.8 \leq D \leq 2$ μm), nanoplankton (f_{nano}; $2 < D \leq 20$ μm), and microplankton (f_{micro}; $20 < D \leq 120$ μm). It is important to emphasize that although we use terminology associated with this planktonic size classification, the measured PSDs in this study encompass all particles suspended in seawater, including non-living particles in addition to living plankton. The fractional contributions of each size class to the total number concentration were calculated according to

$$f_{N,\text{pico}} = \int_{0.8}^{2} N'(D) \, dD \Big/ \int_{0.8}^{D\max} N'(D) \, dD \tag{3a}$$

$$f_{N,\text{nano}} = \int_{2}^{20} N'(D) \, dD \Big/ \int_{0.8}^{D\max} N'(D) \, dD \tag{3b}$$

$$f_{N,\text{micro}} = \int_{20}^{D\max} N'(D) \, dD \Big/ \int_{0.8}^{D\max} N'(D) \, dD \tag{3c}$$

where the subscript N indicates the quantity is derived from the number-based size distribution and the second subscript indicates the size fraction. The contributions of the three size classes to the particle area (f_A) and volume

(f_V) distributions were calculated in an identical manner by replacing $N'(D)$ in Equation 3 with $A'(D)$ and $V'(D)$, respectively. These fractional contributions are closely related to the cumulative distribution functions described above. For example, Equation 3a is equivalent to C_N provided in Equation 2 with an upper integration limit of $D = 2$ μm for the numerator. Similarly, the other size classes can be related to C_N through the relations $f_{N,\text{micro}} = 1 - C_N(D = 20$ μm) and $f_{N,\text{nano}} = C_N(D = 20$ μm) $- C_N(D = 2$ μm).

Another means to characterize the overall size distribution was determined by fitting a power law model to the measured data of the density function of particle number concentration (Equation 1). This calculation was performed as a robust linear regression fit to $\log_{10}$-transformed data of $N'(D)$ and D over the size range $D = 0.8$ μm to D_{max} (see Section 3.4).

2.4. Statistical Analyses

In this study we evaluate the ability of different metrics derived from the measured PSDs to estimate the fractional contributions of the pico-, nano-, and microplankton size classes. The degree of correlation between any two variables was assessed using either the Pearson, r, or Spearman rank, r_s, correlation coefficient. Model parameters were obtained by fitting relationships between these metrics and size class using standard Model I linear regression, or with least squares curve fitting approaches employing the Levenberg-Marquardt algorithm for nonlinear models (Moré, 1978). All model parameterizations were determined using robust fitting with Tukey's bisquare weighting (Beaton & Tukey, 1974).

For each relationship, the goodness-of-fit between the individual observations, O_i, and fitted model predictions, P_i, was characterized through the coefficient of determination r^2. To further assess model performance, scatterplots depicting model-derived versus measured values were subjected to Model II (reduced major axis) regression. We report values for the slope S, intercept I, and Pearson correlation coefficient r resulting from this analysis. Other statistical parameters of model performance include the median values of the ratio of model-derived to measured data, MdR, median values of the model bias, $MdB = \text{median } (P_i - O_i)$, and the median absolute percent difference, $MdAPD = 100 \times \text{median } | (P_i - O_i)/O_i |$, between the model-derived and measured values. The root mean square deviation between model predictions and observations, $RMSD$, is also provided.

3. Results and Discussion

3.1. Estimated Uncertainties in Measurement of the Particle Size Distribution

The relative uncertainty in the measurement of D with a Coulter counter is estimated to be around 0.5% (Jonasz & Fournier, 2007), and this value is consistent with our observations from calibration experiments using NIST-traceable polystyrene bead size standards. Uncertainties in the estimates of particle concentration within each size bin can be partitioned into two inherent sources; counting errors that reflect the subsampling of particles within an inhomogeneous seawater sample, and instrument uncertainties associated with the determination of reference blank, interrogated volume, and particle diameter.

Owing to the relatively dilute concentrations of particles in seawater and practical limitations regarding sample volume and time of measurement, the largest source of uncertainty is usually associated with the counting error. Assuming particles in seawater are distributed according to a Poisson distribution, the relative counting uncertainties associated with subsampling can be approximated as $1/\sqrt{n}$. This indicates that a count of 100 particles is required to achieve an uncertainty level of 10% in each size bin without regard to additional instrument-specific uncertainties. For this study, the combination of interrogated sample volumes and ambient particle concentrations resulted in median particle counts within individual size bins that range from a few to several thousand (Figure 2a). The breaks in the depicted curves at a diameter of around 5 μm occur at the transition between the merged 30 and 200 μm aperture data, reflecting the different sampling volumes of the two apertures. The steep decline in particle concentration with increasing diameter is also seen in the data for each aperture, with some observed peaks associated with persistent particle populations for different cruises. Particle counts generally exceed 100 per bin throughout most of the aperture size range, but despite the aggregation of bins at the upper end of the aperture size ranges lower particle counts are still observed. The pattern among individual cruises is related to a combination of ambient particle concentration and sampling volume. For example, although having generally larger sampling volumes than the other cruises, on average BIOSOPE has the lowest counts per bin for the 30 μm
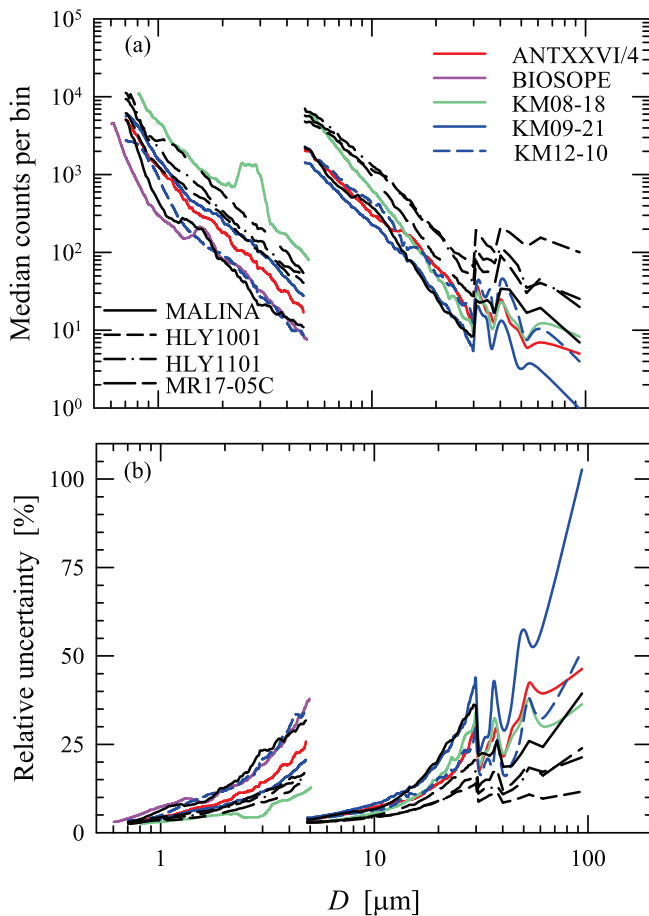
Figure 2. (a) Median number of particles counted as a function of particle equivalent spherical diameter D for Coulter measurements obtained on each cruise as indicated in the legend. Values of D represent the midpoint diameter of each measured size bin. (b) Estimated uncertainty in measurement of particle concentration as a function of D.

aperture (we recall there were no 200 μm aperture measurements on this cruise). In contrast, despite lower sampling volumes the KM08-18 cruise in the SB Channel and the three Arctic cruises on the Chukchi Shelf exhibit the highest average counts in each size bin. The four Arctic cruises also show a tendency for higher particle counts in the larger size ranges.

Blank counts subtracted from each measurement, obtained using seawater from individual sampling locations and filtered multiple times through a 0.2 μm filter, were generally <4% compared to final summed particle counts for $D \leq 1$ μm. Using prior estimates of instrumental error sources associated with the Coulter measurement (Jonasz & Fournier, 2007), we calculated the average relative uncertainty of concentration in each bin using standard propagation of error (Figure 2b). The counting uncertainty dominates the overall uncertainty budget in nearly all bins, and thus the patterns are essentially mirror images of those seen in Figure 2a. The median estimated uncertainty within each size bin ranges from 5% to 11% among cruises, and exceeds 35% for typically less than 5% of the size bins. These latter bins are mostly associated with the size range $D > 30$ μm in the clearest sampled waters where oceanic particle concentrations are very low.

For the BIOSOPE cruise, HIAC data are used for the size range of $D = 5$–100 μm. The HIAC measurements are based on the analysis of four 25 cm³ replicates (Stemmann et al., 2008), with median counts ranging from ~1,200 particles per bin to values <1 for bins in the largest size range. Assuming a similar instrumental uncertainty as the Coulter measurements, average uncertainty estimates range from 4% to 211% among size bins and exhibit a similar pattern of increasing uncertainty with increasing particle size, with values exceeding 50% for the size range $D > 30$ μm.

We note that our uncertainty estimates do not include other potential sources of measurement error, for example possible uncertainties associated with modifications of the particle assemblage during the capture and subsequent withdrawal of seawater during sampling, or particle breakage occurring from shear induced during the Coulter measurement (e.g., Jonasz & Fournier, 2007; McCave, 1984). Such types of uncertainties are strongly dependent on the types and characteristics of the particles present in a given sample, and thus are difficult to quantify on a general basis. Our estimates of uncertainty can thus be considered lower limits, and actual uncertainties may be higher for individual samples.

3.2. General Features of the Particle Size Distribution

Figure 3 illustrates all measured density functions for particle number concentration as a function of particle diameter, $N'(D)$, for both the PacAtl and Arctic datasets. In this combined dataset values of $N'(D)$ at a diameter of 1 μm exhibit more than a 1500-fold range from 1.6×10^9 to 2.5×10^{12} m^{-3} μm^{-1}, consistent with values reported in previous studies (Jonasz & Fournier, 2007). The largest values are associated with coastal environments from the Arctic and KM08-18 cruises, with smaller values typically observed in open ocean waters of the Pacific and Atlantic Oceans. This pattern is similar for values of $N'(D)$ throughout the size range, although for the larger end of the particle size range the Arctic cruises exhibit values of $N'(D)$ noticeably elevated compared to those observed in the PacAtl cruises. For all samples, the values of $N'(D)$ decreased over the entire measured size range with increasing diameter. The values of the slope ζ_N, obtained by fitting each measured $N'(D)$ to Equation 1, range from -4.49 to -2.65 with an average value of -3.58 ± 0.34 and a median value of -3.60 ($n = 394$; Figure 4). These average values and range of variability are in general agreement with previous studies of coastal and oceanic waters reported for different size ranges (Buonassissi & Dierssen, 2010; Jonasz & Fournier, 2007; Reynolds et al., 2010; Xi et al., 2014). No significant difference was observed in the average values of ζ_N between the PacAtl and Arctic datasets, including a comparison restricted to near-surface samples only (ANOVA, $p > 0.05$).
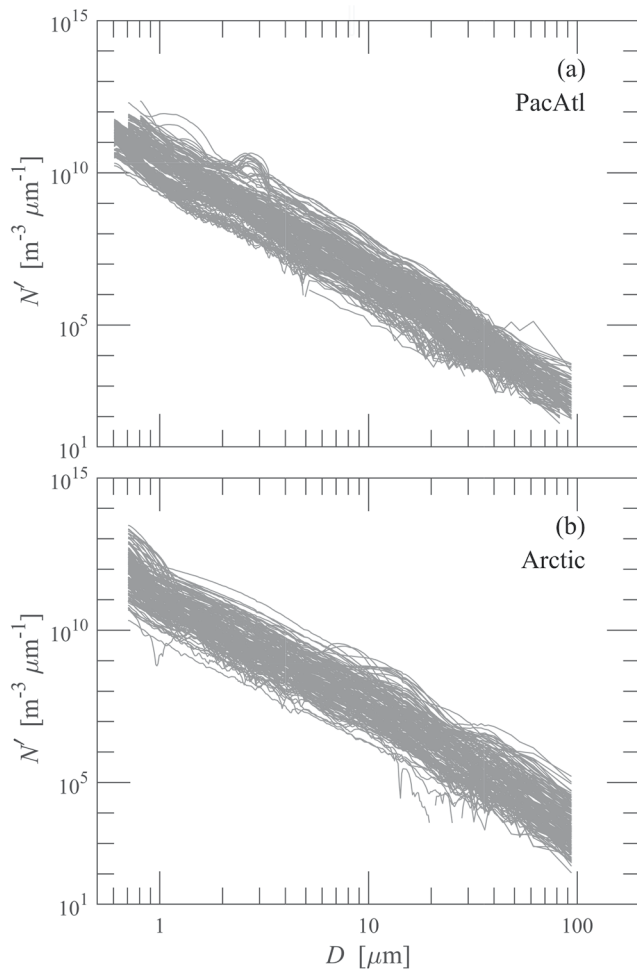
Figure 3. All measured density functions of particle number concentration, N', as a function of particle diameter for the (a) PacAtl and (b) Arctic datasets.
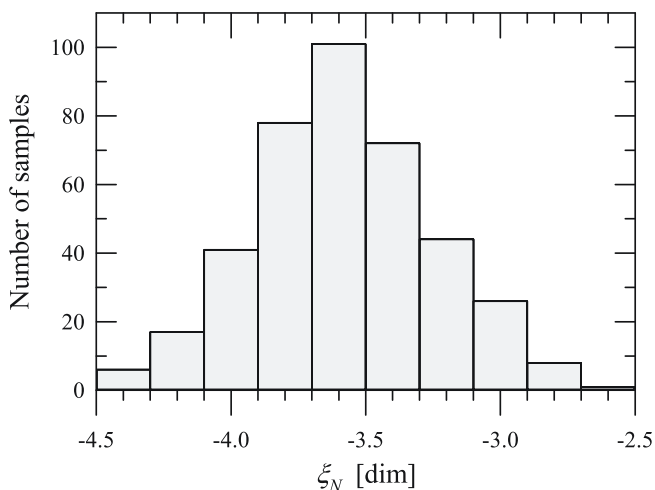

Figure 4. Histogram of the exponent ξ_N obtained by fitting a single-slope power law model (Equation 1) to all 394 measurements of $N'(D)$ in the combined PacAtl and Arctic datasets.

Example measurements of $N'(D)$ at different sampling depths and corresponding fits of the power law model are illustrated for two stations in Figure 5. Note that in this figure, different scaling factors are applied to $N'(D)$ for the samples from subsurface depths in order to improve visualization of the individual measurements. Figure 5a depicts $N'(D)$ measurements at three depths from a BIOSOPE station near the center of the ultraoligotrophic South Pacific Gyre. This location represents one of the lowest surface values of Chla (0.02 mg m^{-3}) in the combined datasets, with a very deep subsurface chlorophyll-a maximum (SCM) of 0.18 mg m^{-3} observed at 175 m. Despite a 9-fold increase in Chla relative to the surface, the integrated particle number concentration over the size range $D = 0.8$–120 μm, N_t, decreased about 18% in the SCM. The fit to the surface values of $N'(D)$ indicates a consistent and increasing overestimation of particles by the power law model for particle diameters exceeding about 5 μm. This overestimation of large particles is not as strong in the sample from the SCM, but the power law model fails to capture prevalent peaks in this PSD occurring at diameters of 0.6, 1.6, and 2.5 μm which are related to the presence of individual planktonic populations. For the sample obtained from the mesopelagic depth of 400 m, N_t has further decreased to 44% of the surface value and the shape of $N'(D)$ is relatively featureless. Of the three measurements, this sample is best represented by the power law model although there remains a tendency to poorly estimate particle concentrations at both the lowest and highest values of particle diameter. At this station, samples from both the SCM and below the mixed layer have a steeper power law slope than observed in the near-surface, −3.7 vs. −3.3, which is a frequently observed trend for many stations within our dataset.

In contrast to the BIOSOPE station in Figure 5a, Figure 5b depicts a northern Chukchi Sea station from the Arctic dataset which has a much higher value of Chla (0.6 mg m^{-3}) in the near-surface layer, with a corresponding increase in total particle number concentration of more than 100-fold. In the SCM at 26 m depth, Chla further increased to a value of 5.5 mg m^{-3} but the value of N_t is only 8% of the surface value. Both of these samples also demonstrate the presence of prominent peaks in the distribution for various regions including the nanoplankton size range, and large overestimates of large particle concentration by the fitted power law model. The deepest sample at 147 m was obtained within 5 m from above the seafloor, and the value of N_t is increased by about 80% relative to the SCM. Ancillary measurements indicate this sample had a very low organic carbon content relative to particle mass concentration, consistent with a predominant presence of resuspended inorganic sedimentary particles. In contrast to the shallower samples, the measured PSD lacks well-defined peaks but exhibits broad changes in the slope of $N'(D)$ across the entire size range which are also poorly reproduced by a single-slope power law model.

3.3. Relative Contributions of Individual Particle Size Classes

For the 226 PSD measurements comprising the PacAtl dataset, values of the total particle number concentration N_t show large differences in the near-surface layer among cruises. By a large extent, the BIOSOPE cruise exhibited the lowest particle concentrations with values of N_t in the surface ranging from 0.39 to 2.47 × 10^{10} m^{-3}, with an average value of 1.09 ± 0.76 × 10^{10} m^{-3}. The highest values were associated with samples from the mesotrophic waters near the Marquesas Islands, with minimum values of N_t observed in the ultra-oligotrophic South Pacific Gyre. In contrast, the highest average surface particle concentration
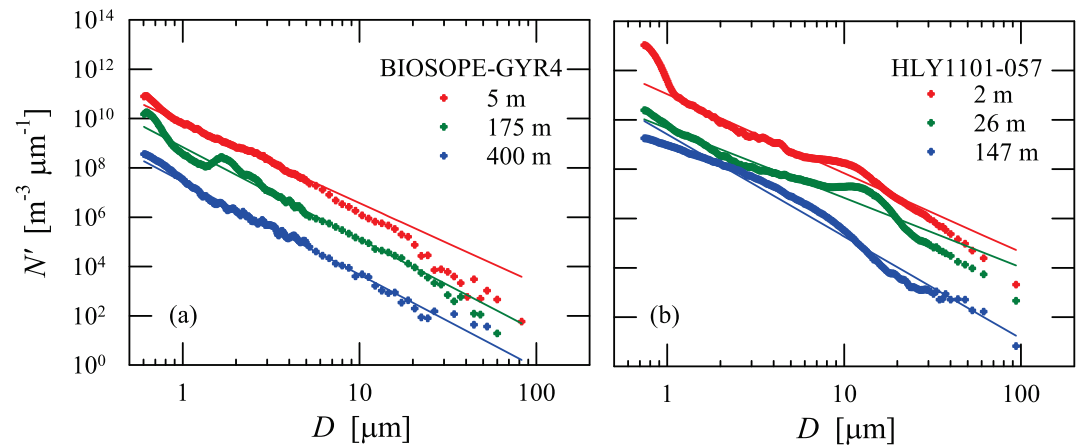
Figure 5. Examples of measured density functions of particle number concentration, $N'(D)$, for two locations in the PacAtl and Arctic datasets. For each individual measurement, the corresponding fit obtained from the power law model is depicted as a solid line. (a) Samples obtained at BIOSOPE station GYR4 for depths corresponding to near-surface (5 m), the subsurface chlorophyll-a maximum (175 m), and from a depth in the mesopelagic zone (400 m). (b) Samples obtained for analogous depths at HLY1101 station 057. In both panels, for visual clarity all values of $N'(D)$ from the subsurface chlorophyll-a maximum have been divided by 10 and all values of $N'(D)$ from the deepest sample have been divided by 100.

$(1.64 \pm 0.55 \times 10^{11} \ \text{m}^{-3})$ was observed for the KM08-18 cruise in coastal waters of the SB Channel. The two Hawaiian cruises (KM09-21, KM12-10) and the ANTXXVI/4 cruise exhibited intermediate surface concentrations between these endpoints, although it is notable that the highest observed surface concentration in the PacAtl dataset $(5.64 \times 10^{11} \ \text{m}^{-3})$ was measured at station 299 of the ANTXXVI/4 cruise off the coast of Brittany. This station was also associated with elevated surface values of Chla $(1.5 \ \text{mg m}^{-3})$ and other measures of particulate mass and organic carbon concentration (Uitz et al., 2015).

For the Arctic dataset, the average value of N_t in surface waters is about 5.5-fold higher than observed in the PacAtl dataset, but has a much smaller range in variability between the four different cruises $(1.57–3.52 \times 10^{11} \ \text{m}^{-3})$. The lowest values of $\sim 2 \times 10^{10} \ \text{m}^{-3}$ were obtained northward of the continental shelf in the relatively clear waters of the Beaufort Sea, with the highest values exceeding $10^{12} \ \text{m}^{-3}$ observed on the shelf both in the vicinity of the Mackenzie River plume and in the Chukchi Sea. Further discussion and additional examples of data from the Arctic dataset are provided in Reynolds et al. (2016) and Runyan et al. (2020).

The cumulative distribution functions of particle number, $C_N(D)$, cross-sectional area, $C_A(D)$, and volume concentration, $C_V(D)$, obtained for all measurements using Equation 2 are depicted in Figure 6. The $C_N(D)$ generally shows a rapid increase with increasing particle diameter as counts of large particles are always very low relative to the number of smaller particles, with 50% or more of the particle number concentration represented by diameters <1.5 µm. In contrast, the $C_A(D)$ and to greater extent the $C_V(D)$ increase less rapidly, and generally exhibit a greater range in the particle diameter associated with a given percentile as specified by a given value of $C_A(D)$ or $C_V(D)$. Compared to the PacAtl dataset, the Arctic data display a larger variability in the shape of these cumulative distributions, with a broader range of particle diameters associated with a given percentile value.

The fractional contribution of the three different planktonic size ranges (f_{pico}, f_{nano}, and f_{micro}) to the summed particle number, cross-sectional area, and volume concentration calculated from the cumulative distribution functions are shown in Figure 7, with Figure 8 depicting a statistical summary of the measurements for the PatAtl and Arctic datasets. There is an overall pattern of increasing contributions from larger particles when moving from the distribution of particle number concentration to distributions of particle area and volume concentration. In accordance with the steep slope of $N'(D)$, the contribution of picoplankton-sized particles overwhelmingly dominates the particle number concentration with values of $f_{N,pico}$ in the combined datasets averaging $89 \pm 4.4\%$ and always greater than 76% (Figure 8a). The corresponding values of $f_{N,nano}$ range from 0.3% to 24%, with $f_{N,micro}$ never exceeding 0.17%. Despite this limited range of $f_{N,micro}$, a statistically significant difference was observed between the two datasets ($p < 0.001$) with the average value for the Arctic about 3-fold higher than the value obtained for the PacAtl dataset.
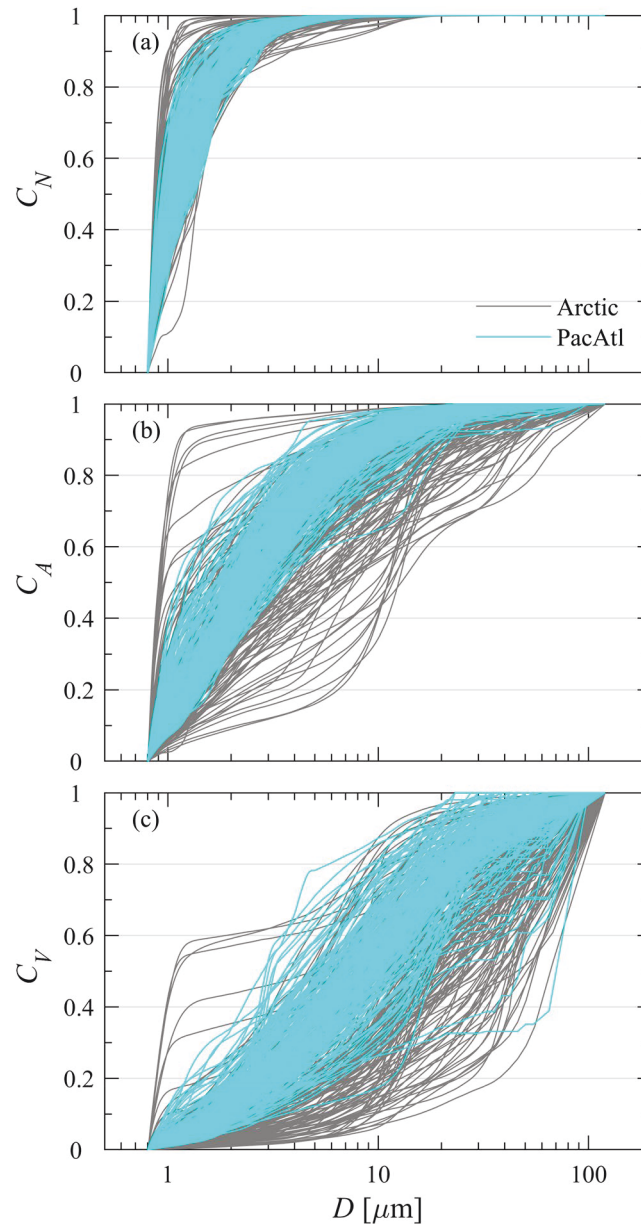
Figure 6. Measured cumulative distribution functions C of particle (a) number, (b) cross-sectional area, and (c) volume concentration for the Arctic and PacAtl datasets. In this figure, the values of D represent the upper limit of each individual size bin.

Comparable contributions from the pico- and nanoplankton size classes on average comprise the dominant contributions to the particle area concentration in both datasets, with both $f_{A,\text{pico}}$ and $f_{A,\text{nano}}$ spanning a broad range (9%–95% and 4%–85%, respectively) (Figure 8b). The microplankton size class again has typically small contributions, with values of $f_{A,\text{micro}}$ averaging $5.4 \pm 5.9\%$ and always <36% for the combined dataset. Similar to $f_{N,\text{micro}}$, the average contributions of the microplankton size class to A_t is about 3-fold higher for the Arctic dataset.

The nanoplankton size class exhibited the largest contribution to particle volume concentration for nearly all PSD measurements in the PacAtl dataset, with an average value of $f_{V,\text{nano}} = 64 + 8.6\%$ and always at least 26% (Figure 8c). Contributions of $f_{V,\text{micro}}$ range from 2% to 67%, but exceeded $f_{V,\text{nano}}$ in only 4 of the 226 measured distributions. In the Arctic dataset, there is almost a twofold increase in the average contribution to particle volume concentration by the microplankton size class compared to the PacAtl dataset, and thus a nearly balanced contribution between these two size classes. In contrast to particle number and area, the picoplankton size fraction
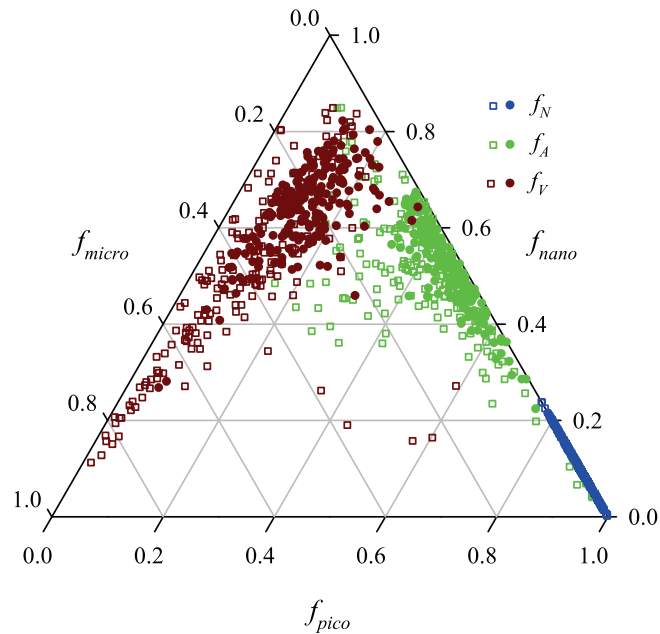
Figure 7. Ternary diagram illustrating the fractional contribution of three discrete particle size classes ($f_{pico}, f_{nano}, f_{micro}$) to the total concentration of particle number, f_N (blue), cross-sectional area, f_A (green), and volume, f_V (red), for the PacAtl (●) and Arctic (□) datasets.

has the smallest average contribution of 12% to particle volume concentration, and had the largest contribution in only four samples from the Arctic.

The fractional contribution of a size class in one distribution of particle size is correlated to a varying degree with its contribution to other distributions (Table 2). These correlations are generally strongest when moving a single "step" in measures of particle size (i.e., from f_N to f_A, or from f_A to f_V) and weakest when moving two steps (i.e., f_N to f_V). For example, the fractional contribution of the picoplankton size class to the total number concentration of particles, $f_{N,pico}$, is reasonably well correlated with its contribution to total particle area $f_{A,pico}$ ($r_s = 0.69$) but to a much lesser extent with its contribution to total particle volume $f_{V,pico}$ ($r_s = 0.28$). The correlation coefficients in Table 2 indicate that translating particle size class contributions from one measure of the particle size distribution to another is not always reliable owing to the convolution of particle number and the area or volume weighting as a function of diameter.

3.4. Estimation of Particle Size Class Contributions From the Power Law Model

We examined how well the single-slope power law approximation to our measurements of the particle number concentration yields the fractional contributions of each size class to total particle number, area, and volume concentrations.

For each PSD, the fitted coefficients of a power law model were obtained through robust linear regression analysis to $\log_{10}$-transformed data of $N'(D)$ and D over the size range $D = 0.8$ μm to D_{max} (Equation 1). The model fitting routine employed bisquare weighting of residuals in $N'(D)$ to minimize the influence of large outliers and yield a robust estimate of the slope across the entire size range (Beaton & Tukey, 1974). Because of the size-dependent changes in uncertainties (Figure 2b), we additionally tested fitting of the power law model using ordinary least squares in which the residuals in $N'(D)$ were weighted by the reciprocal of the squared uncertainty estimates calculated for each pair of D and $N'(D)$. These results indicated comparable results in the calculated regression parameters obtained from the two methods; on average the slope estimate agreed to within 1% (0.8 ± 7.6%) and differences greater than 20% were observed for only 8 of the 394 measured PSDs. The fitted power law model was then used to determine the predicted value of $N'(D)$ for each of the discrete size bins of the original PSD measurement, and the modeled contributions of each size fraction ($f_{N,pico}, f_{N,nano}, f_{N,micro}$) were calculated for com-
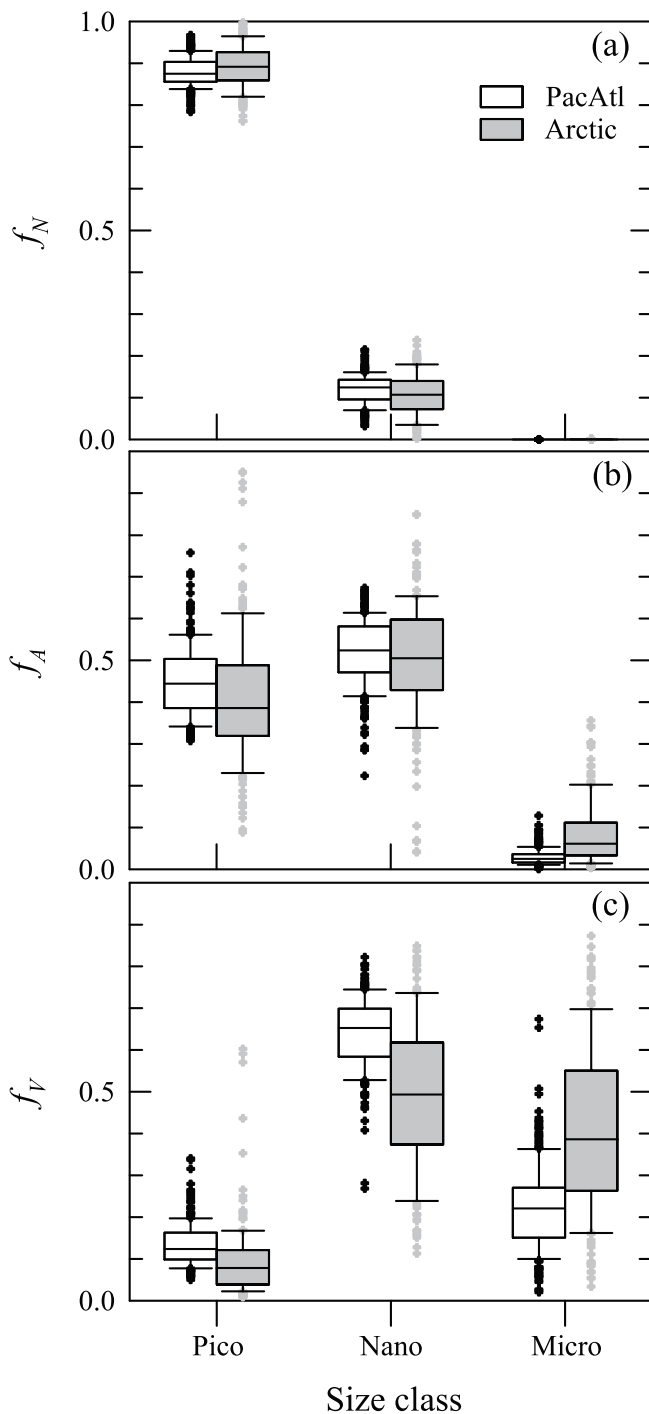
Figure 8. Box and whisker plot summarizing the relative contribution of three discrete particle size classes (pico, nano, micro) to the total concentration of (a) particle number, f_N, (b) cross-sectional area, f_A, and (c) volume, f_V, for the PacAtl and Arctic datasets. Each box depicts the median with boundaries representing the 25th and 75th percentile values, and whiskers indicate values of the 10th and 90th percentiles.

parison with the actual contributions computed from Equation 3 using the measured data. Similar calculations were made on the basis of $A'(D)$ and $V'(D)$ distributions, which provided the comparison for values of $f_{A,\text{pico}}, f_{A,\text{nano}}, f_{A,\text{micro}}$ as well as $f_{V,\text{pico}}, f_{V,\text{nano}}, f_{V,\text{micro}}$.

Scatter plots depicting these comparisons between the modeled and observed size class contributions are illustrated in Figure 9, and Table 3 provides a statistical characterization of these relationships. Overall, the results support a general conclusion that the single-slope power law approximation to oceanic PSDs over the size range examined in this study does not provide reliable estimates of the fractional contributions of pico-, nano-, and microplankton size classes to total particle number, cross-sectional area, or volume concentration. For all relationships only a low to moderate correlation is observed between the values of the predicted size class contribution from the power law model and the actual measurements, with nearly all values of the correlation coefficient r less than 0.6. The highest correlation coefficient is associated with the estimation of $f_{N,\text{micro}}$ for which the measured contribution never exceeds a value of 0.002 (Figure 9c), but these predictions exhibit a large overall bias ($MdR = 1.67$) with an average absolute prediction error that exceeds 66%. These observations of strong bias and high prediction error are increased to an even greater extent in the area and volume relationships for the microplankton size fraction (Table 3). The best performance of the power law in terms of minimal error and bias is the prediction of the contribution of picoplankton size class to the particle number concentration, $f_{N,\text{pico}}$; this represents a case, however, in which the picoplankton contribution is always dominant and the value of $f_{N,\text{pico}}$ varies over a limited range regardless of the power law slope (Figures 8a and 9a). Additionally, the correlation coefficient between the modeled and measured values of $f_{N,pico}$ is very weak ($r = 0.16$) as the modeled values exhibit both considerable scatter around the 1:1 line and systematic biases as indicated by a value of the regression line slope that differ substantially from 1. The contributions of the nanoplankton size class to all three size fractions also exhibit weak to no correlation between modeled and measured values, and in contrast to the microplankton size class the power law model generally yields consistent underestimates of f_{nano} (MdR of 0.63–0.90).

3.5. Estimation of Particle Size Class Contributions From Percentiles of the Cumulative Distribution

In addition to the power law model, non-parametric statistical measures derived from the PSD such as the mean or median particle size are also commonly used as a means to characterize particle size distributions (e.g., Briggs et al., 2013; Slade & Boss, 2015; Woźniak et al., 2010). In our previous analysis of the 168 PSD measurements obtained from Arctic waters (Runyan et al., 2020), we found that median particle size for a given measure of particle size was only weakly correlated with the relative contributions of different particle size classes; however, stronger correlations were noted for other percentile diameters derived from the distributions C_N, C_A, and C_V. Here we extend upon those observations by examining in further detail relationships between individual percentile diameters and relative size class contributions for size distributions of natural oceanic particle assemblages. In this analysis, we examined the combined dataset of 394 PSDs consisting of the 226 PSDs from the PacAtl dataset and the 168 PSDs from the Arctic dataset. The goal of this analysis was to identify a relatively simple set of percentile diameters which can serve as proxies for the contributions of the three particle size classes to diverse particulate assemblages encountered in oceanic waters

Table 2

Spearman Rank Correlation Coefficients r_s for Relationships Between the Fractional Contribution f of Three Particle Size Classes (Pico-, Nano-, Microplankton) to the Total Particle Concentration Between Distributions of Particle Number, N, Cross-Sectional Area, A, and Volume, V, Concentration

Size class	f_A	f_V
Pico		
f_N	0.69	0.28
f_A		0.82
Nano		
f_N	0.83	0.45
f_A		0.56
Micro		
f_N	0.92	0.74
f_A		0.92

Note. The number of observations is 394 representing the combined PacAtl and Arctic datasets.

spanning a range from ultra-oligotrophic subtropical open ocean waters to coastal polar waters in the Arctic.

Figure 10 illustrates values of Spearman's coefficient of rank correlation, r_s, between specific percentile values of the cumulative distribution with the three particle size class contributions for each measure of particle size. For convenience, this figure depicts absolute values of $|r_s|$ but we note that for many relationships the sign of the correlation is negative (i.e., f decreases with increasing percentile diameter). In general, most percentile values of the cumulative distribution exhibit some degree of correlation with size class contributions f but the strength of this correlation varies from essentially zero ($|r_s| = 0.01$) to very high ($|r_s| > 0.95$). There is typically a specific range of percentile values where maximal correlation is observed, and this range varies between size fractions (i.e., for f_{pico}, f_{nano}, f_{micro}) as well as between measures of particle size (i.e., for C_N, C_A, C_V). The median particle size (50th percentile) does not exhibit the maximum correlation in any distribution, and alternative percentiles are observed to display a stronger correlation.

For percentiles derived from the cumulative distribution of particle number concentration, C_N, the contributions of pico- and nanoplankton size classes have an identical pattern in the magnitude of the correlation coefficient but with opposite signs (negative for $f_{N,pico}$, positive for $f_{N,nano}$), and a prominent peak around the 85th percentile diameter (Figure 10a). In this distribution, the correlation coefficient with $f_{N,micro}$ is very low for nearly all percentile diameters and only becomes significant for diameters exceeding the 99th percentile. These results are consistent with the observation that the microplankton size class has a very small contribution to particle number concentration, and that most variability in this distribution is related to varying contributions between the pico- and nanoplankton size classes (Figures 7 and 8a).

The relationships for particle cross-sectional area concentration exhibit relatively broad peaks in correlation for the pico- and nanoplankton size fractions, with the maxima shifted toward lower percentiles relative to the number distribution (Figure 10b). Both exhibit maximal correlation at a diameter corresponding to the 35th to 45th percentile range of C_A, with higher values of $|r_s|$ observed for picoplankton. Similarly, the correlation with the microplankton contribution to area has also shifted toward smaller percentiles with value of $|r_s| > 0.85$ for diameters between the 85th and 99th percentiles.

With regards to particle volume distribution, the highest rank correlation coefficients are associated with the pico- and microphytoplankton size fractions and are shifted toward even smaller percentile values (Figure 10c). The correlation with nanoplankton contribution has a similar pattern as microplankton, but with weaker values of the correlation coefficient.

The Spearman rank correlation coefficient provides a measure of the monotonicity between two variables. We further examined scatter plots of all individual correlations depicted in Figure 10, and observed that in many cases the relationship between size class contribution f and percentile diameter was distinctly nonlinear. Utilizing a combination of the results shown in Figure 10 and visual examination of these scatter plots, we selected the most promising percentile diameters from the cumulative distributions C_N, C_A, and C_V for use in the estimation of the fractional contribution made by each size class to the respective size distribution.

For each measure of particle size (i.e., number, cross-sectional area, or volume), Figure 11 illustrates relationships between each of the three size fractions and a specific percentile diameter derived from the cumulative distribution. The Arctic data generally show a broader variability in both relative size class contributions and in the range of percentile diameters derived from the cumulative distributions, but exhibit a remarkable consistency with the data from the PacAtl dataset. We evaluated several types of model formulations to describe the observed relationships (linear, exponential, power, and polynomials of varying degree), but with one exception a power law function of the form $Y = aX^b + c$ was chosen as the best representative model, where X is the chosen percentile diameter, Y is the predicted size class contribution, and a, b, and c are best-fit coefficients. The sole exception is for the relationship $f_{A,micro}$ vs. $D_A(90)$ (Figure 11f), in which a linear model provided slightly better goodness of fit statistics than the power function. The fitted model to the combined data from both datasets is depicted in
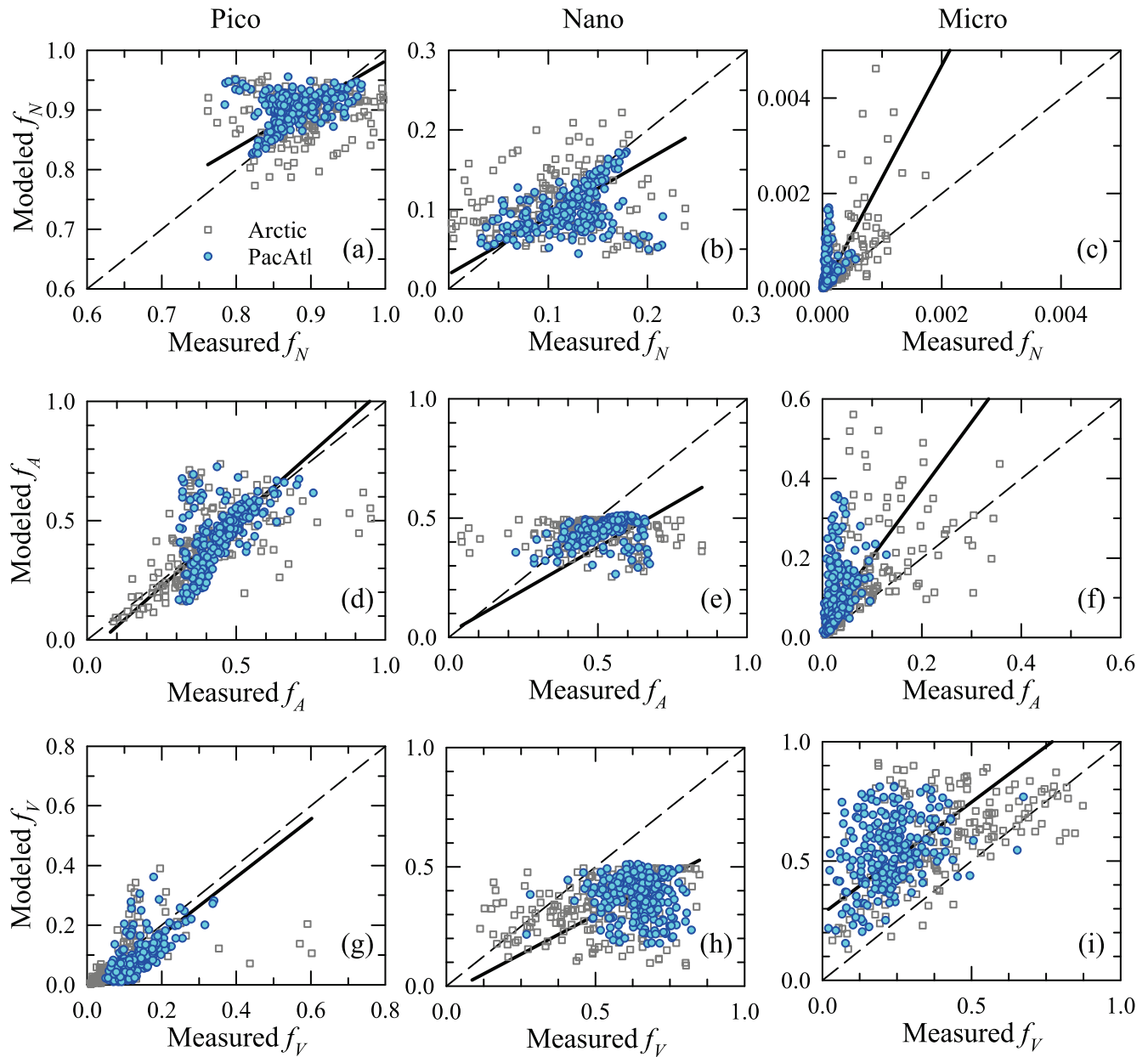
Figure 9. Scatter plots comparing measured values of the fractional contributions of three particle size classes (f_{pico}, f_{nano}, f_{micro}) to modeled values derived from a power law fit to $N'(D)$. (a–c) Fractional contribution to total particle number concentration, f_N. (d–f) Fractional contribution to total particle cross-sectional area concentration, f_A. (g–i) Fractional contribution to total particle volume concentration, f_V. In each panel, the dashed line indicates the 1:1 line and the solid line represents the Model II regression line.

each panel of Figure 11, with the model parameters and statistics characterizing the goodness of fit provided in Table 4. Figure 12 illustrates scatter plots comparing the model predictions with measured values, and statistical descriptors characterizing this aspect of model performance are also given in Table 4.

For the total integrated concentration of particle number, N_t, the diameter corresponding to the 85th percentile of the cumulative distribution C_N, $D_N(85)$, was observed to be a strong predictor of both the pico- and nanoplankton size class contributions in the combined dataset (Figures 11a and 11b). The fitted relationships for these two size fractions with $D_N(85)$ exhibit a very high coefficient of determination ($r^2 = 0.98$; Table 4), and are essentially mirror images of one another in a manner consistent with the dominant contributions of these two size fractions to N_t (Figures 7 and 8a). The power law function provides a very good representation of these relationships, as

Table 3

Statistical Characterization of the Performance of a Single-Slope Power Law Model in Estimating the Fractional Contribution f of Three Size Classes (Pico-, Nano-, Microplankton) to the Total Concentration of Particle Number, N, Cross-Sectional Area, A, and Volume, V

Size fraction	S	I	r	MdR	MdB (dim)	$MdAPD$ (%)	$RMSD$ (dim)
$f_{N,pico}$	0.73	0.25	0.16	1.01	0.01	3.1	0.05
$f_{N,nano}$	0.72	0.02	0.15	0.90	−0.01	26.1	0.05
$f_{N,micro}$	2.35	<0.01	0.66	1.67	<0.01	66.8	<0.01
$f_{A,pico}$	1.11	−0.05	0.57	0.98	−0.01	13.5	0.12
$f_{A,nano}$	0.49	0.20	0.15	0.89	−0.06	13.7	0.13
$f_{A,micro}$	1.69	0.03	0.51	2.22	0.04	122.2	0.11
$f_{V,pico}$	0.97	−0.03	0.55	0.66	−0.03	41.2	0.07
$f_{V,nano}$	0.66	−0.03	0.23	0.63	−0.23	38.0	0.28
$f_{V,micro}$	0.94	0.28	0.47	1.99	0.24	98.6	0.31

Note. All comparisons are based on $n = 394$ measurements of the particle size distribution from the combined PacAtl and Arctic datasets. Modeled values were determined by fitting the measured size distribution to a single-slope power law function (Equation 1) and calculating the resulting contribution of each size class. The slope S, intercept I, and correlation coefficient r of a Model II linear regression between modeled and measured variables is provided. Other statistical metrics include the median ratio, MdR, median bias, MdB, and median absolute percent difference, $MdAPD$, between modeled and measured values. $RMSD$ is the root mean square deviation.

evidenced by low estimates of overall model bias (S and MdR close to 1, MdB <1 × 10⁻³) and accuracy ($MdAPD$ <3.5%). The contribution of the microplankton size class to N_t is always <0.2% for this combined dataset, but despite this limited dynamic range a strong relationship was observed for very high percentile values of D_N, with the percentile diameter representing the 99.9th percentile of this distribution exhibiting the strongest correlation (Figure 11c). The statistics characterizing model performance are poorer compared to the other two size fractions but still reasonably good (Table 4).

In contrast to N_t, the concentration of particle cross-sectional area exhibits less dominance by a single size fraction with comparable average contributions to A_t observed for both the pico- and nanoplankton size fractions (43 ± 12% and 51 ± 11%, respectively). A power function using the 40th percentile diameter $D_A(40)$ of C_A provides a reasonable description of the variable contributions of these two fractions (Figures 11d and 11e), although increasing scatter is observed with increasing $D_A(40)$. The microplankton contribution to A_t is increased relative to N_t with an average value of 5%, but is observed to reach values exceeding 25% in some Arctic measurements. The 90th percentile diameter of C_A is well correlated with $f_{A,micro}$ (Figure 11f), and this relationship also exhibits less pronounced curvature as observed for other relationships. A simple linear model was chosen as it provides slightly better statistical fit than a power function for this relationship. The overall performance of these three model relationships in terms of bias and accuracy is reasonable (MdR 1.00–1.07, $MdAPD$ 3.11%–18.5%) despite increasing scatter observed for larger values of each of the two percentile diameters (Table 4, Figure 12f).

For most measured size distributions in the combined dataset the nanoplankton size class had the largest contribution to the concentration of particle volume, with an average value of $f_{V,nano}$ of 57.8 ± 15.1%. This was particularly true for the lower latitude data from this study, in which the nanoplankton size class was the largest contributor in 222 of the 226 measured size distributions. The microplankton size class was observed to be the dominant contributor to V_t on a more frequent basis in the Arctic observations (60 of the 168 PSDs), particularly for samples where concentrations of chlorophyll-a exceeded 0.5 mg m⁻³. The summed contributions of nano- and microplankton size fractions generally comprise more than 85% of the contribution to particle volume concentration, and both exhibit a strong but opposite correlation with the 60th percentile diameter of C_V (Figures 11h and 11i). The picoplankton contribution to V_t averaged only 12 ± 7.3% for the entire dataset, and was the largest contributor in only four Arctic samples which were influenced by fresh water from either sea-ice melt or river sources, and had notable contributions of inorganic particles as evidenced by a low particulate organic carbon concentration relative to total particle mass concentration. The power function fits for all three size fractions in C_V exhibit relatively low bias with typical errors of <10% (Table 4).

The sum of the three size fractions (i.e., $f_{pico} + f_{nano} + f_{micro}$) in each of the three cumulative distributions C_N, C_A, C_V must equal 100%, and this equality provides an additional means to test the coherence of the individual formulations of each size fraction. Despite use of a separate model parameterization for each of the three size fractions which involve two independent percentile diameters derived from the cumulative distributions, we confirmed that overall model "closure" was very good in each of the three measures of particle size. The best results were observed for the summed fractional contribution of the three size classes to N_t, with an average value of 100.0 ± 0.03% obtained for the 394 observations. The summed contributions to A_t (101.2 ± 5.32%) and V_t (100.4 ± 5.78%) exhibited a larger range but average values were similarly close to 100%.

In all three measures of particle size, two size classes shared a single percentile diameter exhibiting a strong correlation while the third size class had strongest correlation with a different percentile value. For contributions to N_t and A_t, both pico- and nanoplankton size class share a similar predictive percentile, while for V_t the nano- and microplankton share a common percentile diameter. Figure 13 illustrates the frequency distributions of the percentile diameters chosen for the models in Figure 11. Two features are noted for these best-performing percentile
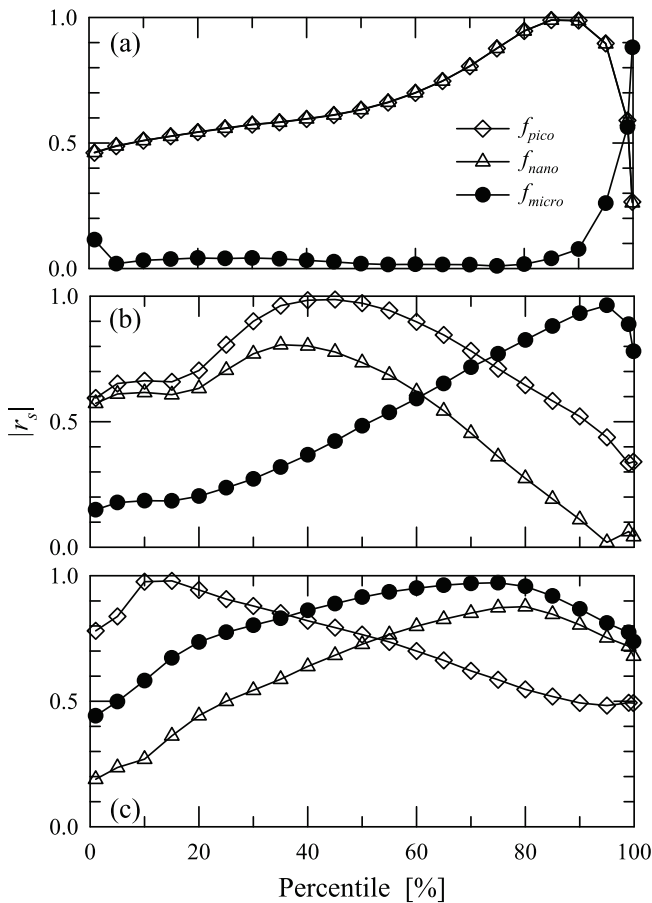
Figure 10. Absolute values of the Spearman rank correlation coefficient r_s for relationships between the fractional contribution of three discrete particle size classes (f_{pico}, f_{nano}, f_{micro}) and different percentiles of the cumulative particle size distribution. (a) $|r_s|$ between f_N and percentiles of C_N. (b) $|r_s|$ between f_A and percentiles of C_A. (c) $|r_s|$ between f_V and percentiles of C_V.

diameters; first, these percentiles exhibit a substantial range of variability in diameter among PSDs in the cumulative distributions (Figure 6). Second, the frequency distribution of these percentiles generally peak near and straddle the diameters used to demarcate one size fraction from another, and decrease as these values move further away from these limits. For example, the two percentiles used to estimate f_{pico} and f_{nano} in the number and area distributions, $D_N(85)$ and $D_A(40)$, had respective mean values of 1.8 ± 0.30 μm and 2.1 ± 1.27 μm that closely match the diameter of 2 μm used to define the boundary between the pico- and nanoplankton size range (Figures 13a and 13b). A similar result is observed for the percentile $D_V(60)$ used to estimate both f_{nano} and f_{micro} in the volume distribution, in which the mean value of 17.6 ± 12.52 μm encompasses the boundary of 20 μm that separates the nano- and microplankton size range (Figure 13c). These results suggest that the choice of predictive percentile diameters may differ for other combinations of PSD size ranges or desired size intervals for prediction.

3.6. Evaluation of Percentile Models With Independent Measurements

We evaluated the relationships developed from the combined dataset (Figure 11) with an independent set of 134 particle size distribution measurements described in Organelli et al. (2018, 2020) and publicly available through the British Oceanographic Data Centre (doi:10/cwbj, accessed December 30, 2020). These measurements were collected on discrete water samples from the upper 500 m of the water column during an Atlantic Meridional Transect cruise from September 27 to October 22, 2016 (AMT26). Particle size distributions were measured with a Multisizer III Coulter counter (Beckman Coulter) using a combination of 20 and 100 μm apertures, which after merging yielded measurements of the PSD over the size range $D = 0.588$–60 μm. For consistency with our measurements, we truncated this data to a lower limit of $D = 0.8$ μm, but it is important to recognize that the upper limit of 60 μm is considerably smaller than that utilized in our study. No additional smoothing or rebinning was applied to these measurements.

The cumulative distributions C_N, C_A, and C_V and the fractional contributions f_{pico}, f_{nano}, and f_{micro} of the three size classes to total concentration were calculated in the same manner as described earlier, with the exception that the value of D_{max} in Equations 2 and 3 is equal to 60 μm. The percentile diameters $D_N(85)$, $D_N(99.9)$, $D_A(40)$, $D_A(90)$, $D_V(20)$, and $D_V(60)$ were derived from the relevant cumulative distributions and used to predict the size class contributions to each distribution using the modeled relationships described in Table 4.

In addition to the Arctic and PacAtl datasets used to parameterize the models, Figure 12 also depicts the comparison of model predictions with actual values calculated from the cumulative distributions for the AMT26 cruise. Despite the difference in measured size ranges, these comparisons for the AMT26 data indicate a very high correlation with values of r generally >0.85. The majority of predicted values fall near the 1:1 line with the observations, and are also consistent with the performance of the model for this study of PacAtl and Arctic datasets.

Statistically, the best results for AMT26 are obtained for the calculations associated with the particle number concentration (Figures 12a–12c). For the pico- and nanoplankton size classes, predicted contributions using the percentile diameter $D_N(85)$ exhibit low average bias ($S = 1.06$, $MdR = 1.00$) as well as very good accuracy ($MdAPD = 0.5\%$). Some systematic bias is suggested, however, in the region where values of $f_{N,pico}$ approach the observed minimum below 0.8 and corresponding $f_{N,nano}$ values exceed approximately 0.2. We note that 4 of the 134 measured size distributions from AMT26 had no counts in the size range $D > 20$ μm, and thus the calculated values of $f_{N,micro}$ are zero in these distributions. For the remaining PSDs, the model predictions of $f_{N,micro}$ using the percentile diameter $D_N(99.9)$ are consistent with our observations and have comparable error statistics.
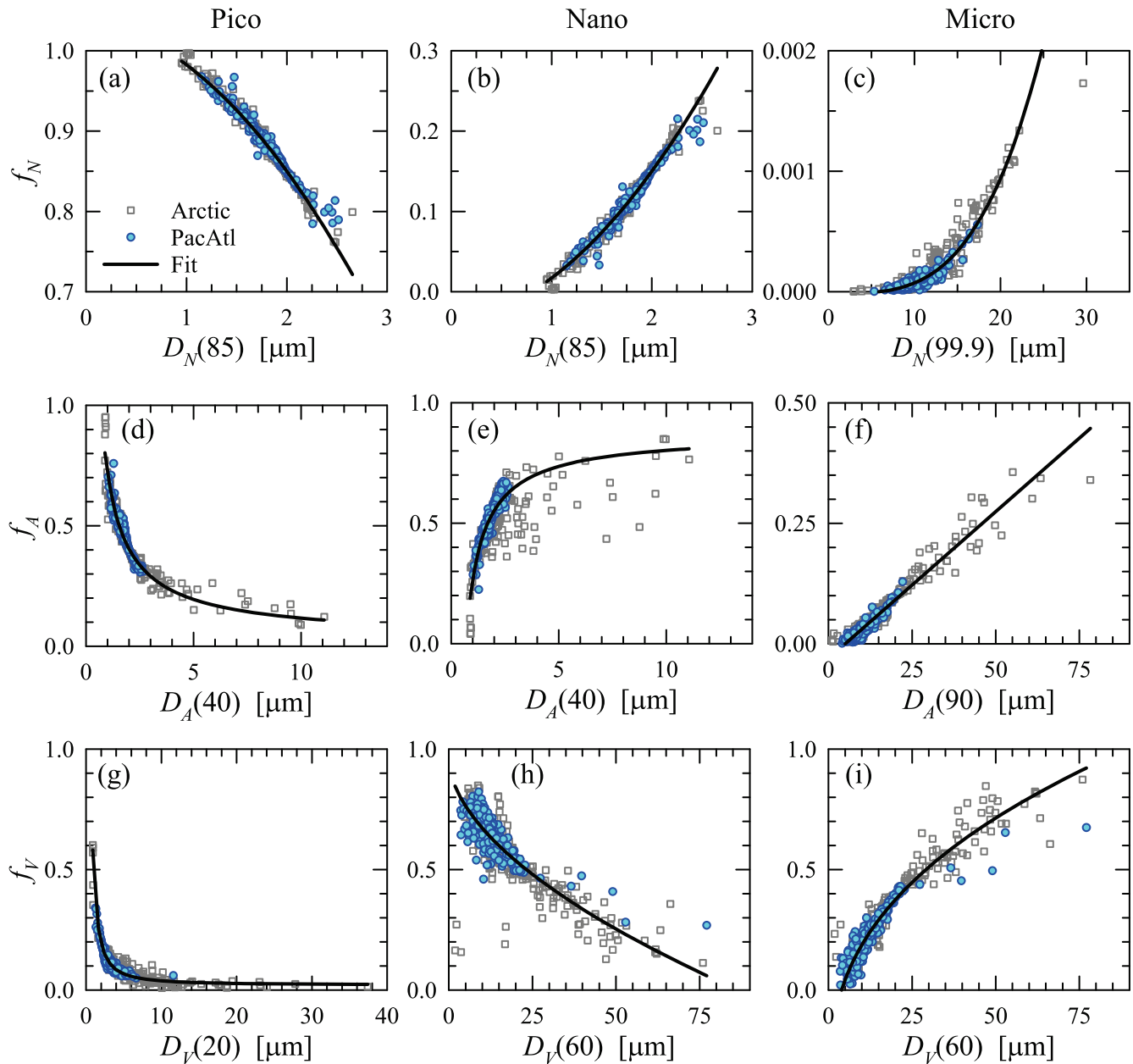
Figure 11. Relationships between specific percentiles of the particle size distribution (PSD) and the fractional contribution of three discrete particle size classes (f_{pico}, f_{nano}, f_{micro}) to the entire distribution for data from the Arctic ($n = 168$) and PacAtl ($n = 226$) datasets. (a–c) Fractional contribution to total particle number concentration as a function of the particle diameter representing the 85th, $D_N(85)$, or 99.9th, $D_N(99.9)$, percentile value of C_N. (d–f) Fractional contribution to total particle cross-sectional area concentration as a function of the 40th or 90th percentile particle diameter of C_A. (g–i) Fractional contribution to total particle volume concentration as a function of the 20th or 60th percentile particle diameter of C_V. The solid line in each panel depicts a fitted power function to the relationship, with the exception of panel (f) in which a linear function is shown.

Model performance with the AMT26 dataset is also reasonably good for the particle cross-sectional area and volume distributions, with predicted values clustering near the 1:1 line and falling within the cloud of data points representing the current study (Figures 12d–12i). The tendency observed in the predicted values of $f_{N,pico}$ and $f_{N,nano}$ toward increased bias near the limits of the observational range are still evident in both f_A and f_V, but with an opposite pattern. Values of S for the regression between modeled and observed values are much less than 1, but the *MdAPD* is still <10% for predictions of pico- and nanoplankton contributions to these distributions. The *MdAPD* for the prediction of the microplankton fraction is increased to about 25%, and also shows some patterns of bias.

Table 4
Parameterization and Evaluation of Models Utilizing Percentile Diameters Derived From the Cumulative Particle Size Distributions to Estimate Fractional Contributions f of Three Individual Particle Size Classes (Pico-, Nano-, Microplankton) to the Total Particle Number, N, Cross-Sectional Area, A, or Volume, V, Concentration

Size fraction (dim)	Percentile diameter (μm)	Model parameters[a]				Model evaluation[b]						
		a	b	c	r^2	S	I	r	MdR	MdB (dim)	$MdAPD$ (%)	$RMSD$ (dim)
$f_{N,pico}$	$D_N(85)$	-0.049	1.889	1.032	0.98	1.019	-0.018	0.98	1.00	0.0003	0.39	0.009
$f_{N,nano}$	$D_N(85)$	0.049	1.889	-0.032	0.98	1.020	-0.001	0.98	1.06	-0.0003	3.22	0.009
$f_{N,micro}$	$D_N(99.9)$	2.935×10^{-8}	3.468	-1.35×10^{-5}	0.96	1.175	-0.0003	0.91	1.08	-2.18×10^{-6}	28.7	<0.001
$f_{A,pico}$	$D_A(40)$	0.692	-0.868	0.023	0.96	0.963	0.014	0.96	1.00	0.0032	3.11	0.035
$f_{A,nano}$	$D_A(40)$	-0.609	-0.906	0.878	0.86	0.960	0.035	0.83	1.07	-0.0006	5.08	0.066
$f_{A,micro}$ [c]	$D_A(90)$	0.006	-0.031		0.97	0.993	-0.0001	0.97	1.01	<0.0005	18.5	0.015
$f_{V,pico}$	$D_V(20)$	0.466	-1.440	0.021	0.96	1.048	-0.006	0.96	1.06	-0.0014	9.30	0.021
$f_{V,nano}$	$D_V(60)$	-0.079	0.561	0.958	0.83	0.902	0.062	0.82	1.05	-0.0006	6.93	0.088
$f_{V,micro}$	$D_V(60)$	0.250	0.387	-0.422	0.94	1.009	-0.004	0.95	1.04	-0.0021	8.62	0.056

Note. All results are based on n = 394 measurements.

[a]Model parameters represent the fitted coefficients of a power function $Y = a X^b + c$, where X is the percentile diameter and Y is the size fraction as indicated in each row. The coefficient of determination r^2 for the fitted model is also provided. [b]The statistical metrics used to characterize model performance are described in Table 3. [c]For this relationship only, a linear model of the form $Y = aX + b$ is used instead of a power function.

The indications of small bias around the 1:1 line seen in the AMT26 data are also observed for some of the individual cruises in the PacAtl dataset. For example, the results from the BIOSOPE measurements exhibit very similar patterns around the 1:1 line as those observed for AMT26. The measurements from the KM08-18 cruise also exhibit some noticeable trends along the 1:1 line, but the pattern of points is different from either the AMT26 or BIOSOPE results. It is also worth noting that these cruise-to-cruise differences are generally not observed in the Arctic dataset, which may result from the limited geographical area of sampling as well as an overall wider dynamic range of observations relative to most of the individual cruises from the PacAtl dataset. Although the observed patterns lead to some small and differing trends in model bias and performance among individual cruises, the overall prediction error is still relatively small. Such cruise-specific patterns are likely unavoidable when attempting to formulate a single general model that is applicable to a wide variety of particle assemblages sampled from multiple oceanic regions, as is the goal of the present study. Despite these observations, our results suggest that these models have potentially broad application with acceptable levels of uncertainty in terms of capturing the relative contributions of individual size fractions over a diverse range of environments.

As the AMT26 measurements have a much smaller upper size limit compared to the cruises in the PacAtl and Arctic datasets, we also examined the potential impact of this reduced size range on model performance through a simple sensitivity analysis. In this exercise, the upper limit D_{max} of the measured size distributions from the PacAtl dataset was truncated to a value of 60 μm, and the resulting cumulative distribution functions, percentile diameters, and fractional size class contributions were recomputed for each PSD. These new values were then compared with the values calculated from the original size range. Briefly, the overall influence on values of percentile diameters and size class contributions when truncating the upper size limit from 120 to 60 μm was generally small. The percentile diameters derived from the cumulative distributions naturally shift toward smaller values, but for the percentiles used in the models depicted in Figure 11 the median decrease is <0.05% for values of $D_N(85)$ and $D_N(99.9)$ to as high as 9% for $D_V(60)$. With regards to the individual size class contributions, as expected the largest impacts are observed for the microplankton size fraction and the degree of change increases progressing from the number to volume distribution. There is a reduction in the average contribution of f_{micro} for each measure of particle size, ranging from -1.8% for $f_{N,micro}$ to -20% for $f_{V,micro}$. These decreases are mirrored by corresponding increases in both the pico- and nanoplankton size classes in each distribution.

We further tested the sensitivity in the predictions of individual size class contributions when percentile diameters determined from the truncated size distributions were used as input to the original model formulations provided in Figure 11 and Table 4. The comparisons of model predictions between these two inputs also suggest rather minor changes in the predicted size fractions, consistent with the generally small changes noted above
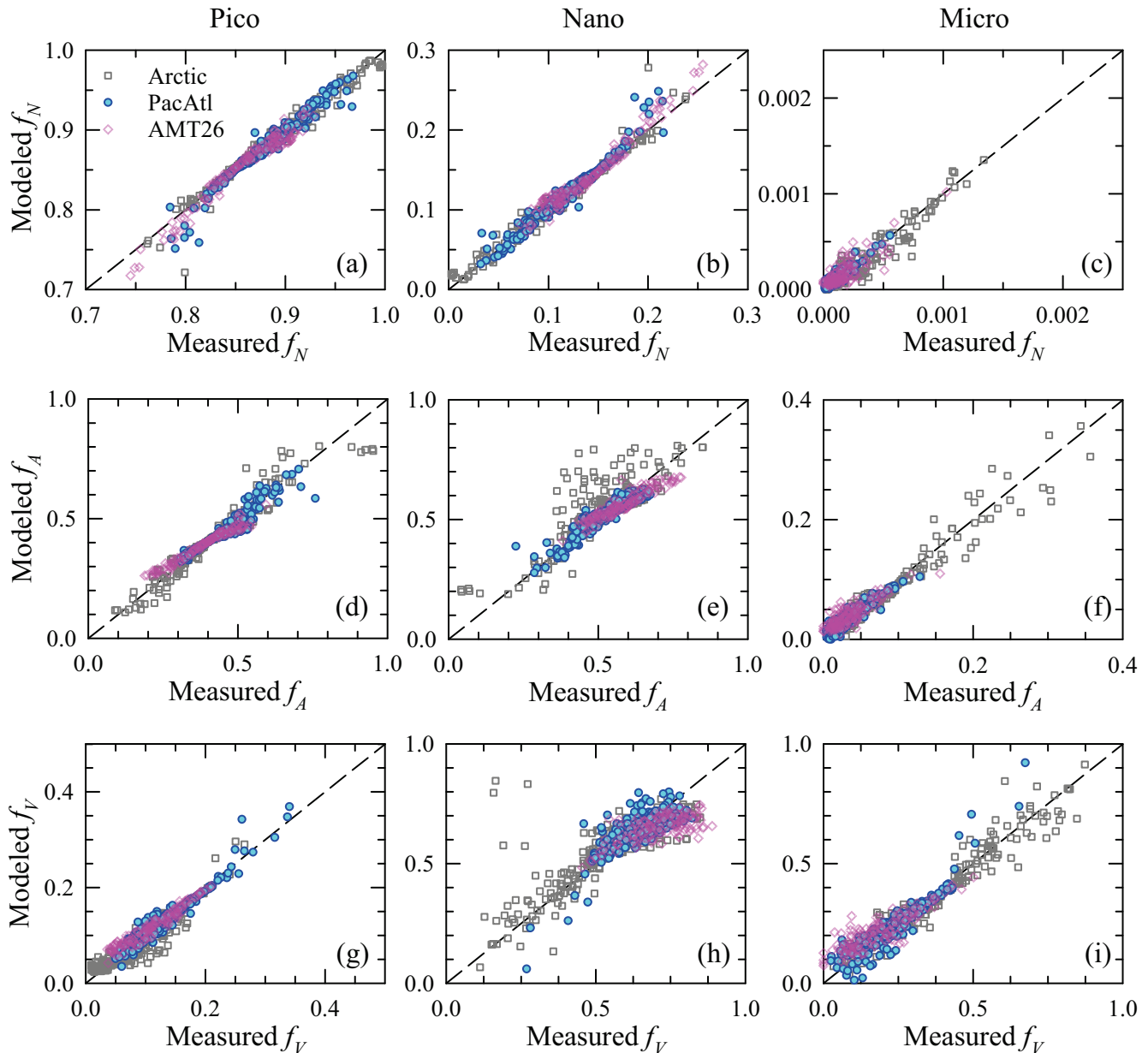
Figure 12. Scatter plots comparing measured values of the fractional contributions of three particle size classes (f_{pico}, f_{nano}, f_{micro}) to modeled values derived from the percentile models depicted in Figure 11. (a–c) Fractional contribution to total particle number concentration, f_N. (d–f) Fractional contribution to total particle cross-sectional area concentration, f_A. (g–i) Fractional contribution to total particle volume concentration, f_V. In each panel, results are illustrated for data from the Arctic ($n = 168$) and PacAtl ($n = 226$) datasets, as well as the independent dataset AMT26 from the study of Organelli et al., 2020 ($n = 134$; measurement range $D = 0.8$–60 μm). The dashed line indicates the 1:1 line in all panels.

regarding the effect on the percentile diameters determined from the truncated cumulative distributions. The observed changes in the predicted size fractions follow the patterns observed in these percentile diameters, with changes in the predicted microplankton size class always the largest within a given distribution, and the degree of change increasing from distributions of particle number to particle volume concentration. For calculated values of f_N and f_A, the median increase in the pico- and nanoplankton contributions are <0.2% and are still ≤5% for f_V. The observed decreases in the microplankton contributions are larger, ranging from −0.2% in f_N to −10% in f_V, although values approaching 100% are observed for some individual PSDs.
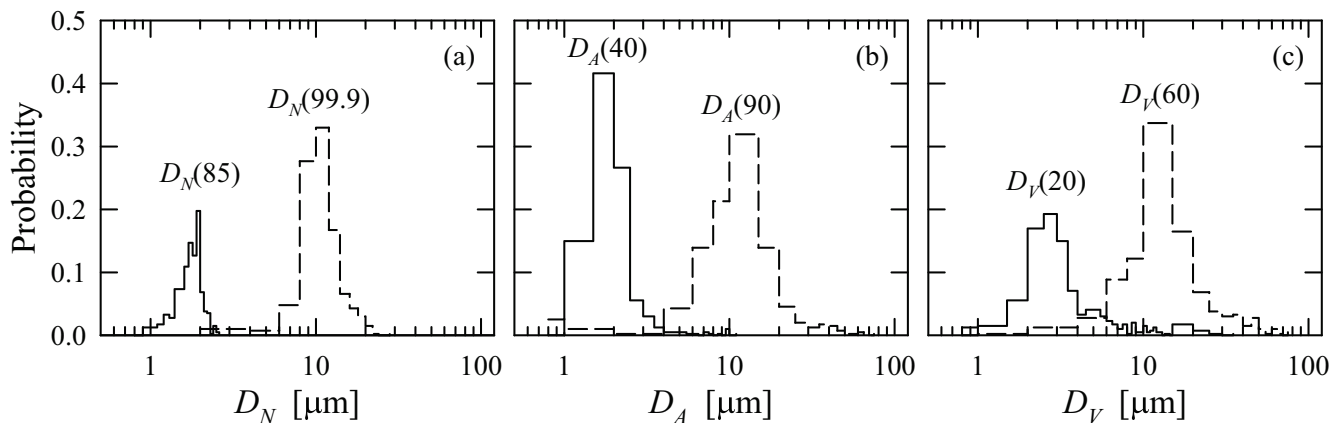
Figure 13. Frequency distributions of the percentile diameters illustrated in Figure 11. (a) Percentile diameters $D_N(85)$ and $D_N(99.9)$ from measured cumulative distributions $C_N(D)$. (b) Percentile diameters $D_A(40)$ and $D_A(90)$ from measured cumulative distributions $C_A(D)$. (c) Percentile diameters $D_V(20)$ and $D_V(60)$ from measured cumulative distributions $C_V(D)$.

In summary, the comparisons between results from both the original and truncated PSDs from the PacAtl dataset suggest that our models based on specific percentiles from the cumulative distributions of particle size are not strongly sensitive to the upper measurement limit of particle size. This is consistent with the observation of generally low particle counts in the size range 60–120 μm for most of the measured PSDs in the PacAtl dataset. We caution, however, that larger changes can be observed for individual PSDs, and thus this conclusion can alter depending upon the changes in the measurement size range as well as the typical shapes of the PSD within a given dataset.

4. Conclusions

Particle size distributions obtained from field measurements in the Pacific, Atlantic, and Arctic Oceans demonstrate substantial changes in both the magnitude and shape among different marine environments, geographically as well as for samples obtained at a single location but at different depths from within the water column. In general, these observations suggest a much larger degree of variability within the Arctic dataset, which likely reflects to some extent the locations of cruises and time periods of sampling. The majority of observations from the PacAtl dataset are from the pelagic ocean and there are relatively few coastal water measurements, and thus the range of variability for these lower latitude coastal regions is likely underrepresented.

It is also important to emphasize that the particle size measurements utilized in this study are limited to a finite range of particle diameters spanning the range 0.8–120 μm. Although this size interval encompasses a broad range of microbial plankton it omits the contribution of some of the smallest planktonic taxa, nor does it assess the role of submicron colloidal materials and nanoparticles which are known to be the most abundant particles in aquatic ecosystems (e.g., Koike et al., 1990; Wells & Goldberg, 1991). Furthermore, the measurement uncertainties in our study increase as the upper limit of the measured size range is approached, and larger particles beyond this limit (e.g., plankton chains or colonies, particle aggregates) are missing from our analyses. Such particles on either end of this size range make a variable but potentially significant contribution to particle concentration in oceanic environments. We also recognize that many oceanic particles exhibit a variety of complex shapes and morphologies, which violates the assumption of sphericity involved in the particle sizing techniques used in this study. The overall uncertainties arising from these different limitations will depend on the particle assemblage, and thus will vary among environments. We note, however, that the broad range of samples represented in our dataset, spanning the pelagic open ocean to turbid coastal regions, likely encompasses the typical diversity of suspended particle assemblages encountered in many marine habitats. Despite this diversity, the relationships based on specific percentile diameters of the cumulative size distributions appear remarkably consistent across the entire dataset. This observation suggests that these percentile-based models capture to a large extent the first order variability pertaining to the shape of the PSD, and that additional complexities related to variations in the

composition and shape of the suspended particles likely contribute to the relatively small scatter observed among individual samples or between marine environments.

The variations in the shape of the PSD for these different environments result in substantial differences in the partitioning of the contributions of individual size intervals to the integrated particle number, cross-sectional area, and volume concentration. We reiterate that while the size classes chosen for this study are based on traditional size classifications of oceanic plankton (i.e., pico-, nano-, and microplankton), our measurements and analyses represent the entire suspended particle assemblage of seawater which includes living and nonliving particles, and both organic and minerogenic material. Because of the strong decrease in the number of particles per unit volume with increasing particle diameter, the contribution of particles in the picoplankton size range to the total number concentration of particles is always high, generally greater than 89%, with only small contributions from larger particles. The size distributions based on particle cross-sectional area and volume exhibit an increasing role of both the nano- and microplankton size classes at the expense of a decreasing contribution of the picoplankton size class, with the nanoplankton size class on average representing the largest contribution to these two distributions. Our results also suggest a significantly greater contribution to particle size from the microplankton size class in Arctic waters compared to the observations from the PacAtl dataset. The ability to quantify and monitor such changes in the partitioning of relative contributions among various particle size intervals has important implications for understanding size-dependent biogeochemical and ecological processes in the ocean.

Parametric descriptions of the oceanic PSD, such as the power law or similar models, provide a simple means to describe the general shape of the PSD in aquatic ecosystems. These formulations are convenient for numerical modeling, and often have some general theoretical basis. Our field measurements indicate, however, that while a single-slope power law model describes the overall general trend of the PSD over a given size range, its predictive capabilities for natural marine particle assemblages is poor owing to frequent and significant departures from the assumption of a single slope throughout the entire size range. The high size resolution measurements obtained with the Coulter counter reveal the common occurrence of peaks in the distribution that are associated with specific planktonic populations, as well as broader changes in the slope of the size distribution occurring over the entire range. These departures from an idealized single-slope power law parameterization have been noted in numerous field studies (e.g., Jonasz & Fournier, 1996; Organelli et al., 2020; Reynolds et al., 2010, 2016). As a consequence, application of the power law model can yield considerable inaccuracies in predicting how the total particle concentration is partitioned among individual size classes.

The mean or median particle size calculated over a given size range is also commonly employed as a single metric to quantify changes in the shape of the PSD (Bernard et al., 2007; Briggs et al., 2013; Slade & Boss, 2015; Woźniak et al., 2010). Our results indicate that the median particle diameter is generally a poor predictor of the individual contributions for the three size classes examined in this study, but we did observe strong correlations between these size class contributions and other percentile diameters derived from the cumulative size distributions. The percentile diameters that displayed the best performance in predicting the pico-, nano-, and microplankton size class contributions (i.e., f_{pico}, f_{nano}, f_{micro}, respectively) varied between the 20th and 99.9th percentiles depending on the measure of particle size (i.e., number, cross-sectional area, or volume) and the given size class. These percentile diameters exhibited the common characteristic of having both considerable variation in the values observed among individual PSDs and a frequency distribution which encompassed one of the diameters used to delineate the individual size classes. An important advantage of this approach based on these non-parametric descriptors of the cumulative size distribution is that they require no assumption regarding the underlying shape of the PSD. Our results also suggest that these models are relatively robust for a variety of sampling locations and diverse types of particle assemblages, and are not strongly sensitive to small alterations in the measured size range.

For each cumulative distribution of particle size, we observed that two of the three size classes shared a common percentile diameter with strong predictive capabilities. A single 85th percentile diameter, $D_N(85)$, based on the particle number distribution allowed the estimation of the pico- and nanoplankton contributions to particle number concentration. A single 40th percentile diameter, $D_A(40)$, based on particle cross-sectional area distribution provided a good proxy for the pico- and nanoplankton contributions to particle cross-sectional area concentration. Finally, both the nano- and microplankton contributions to particle volume concentration could be determined from the 60th percentile diameter, $D_V(60)$, based on the particle volume distribution. In each case the remaining contribution by the third size class can be readily calculated as $1 - (f_1 + f_2)$, where f_1 and f_2 are the two estimated

fractional contributions, so it is feasible to use a single percentile diameter to partition the entire size distribution into the three classes.

Because of fundamental linkages between the optical properties of a particle suspension and the size distribution of the suspended particles (e.g., Morel & Bricaud, 1986; Stemmann & Boss, 2012; Stramski & Kiefer, 1991), it is conceivable that the percentile diameters from the cumulative size distributions can be reasonably estimated from measurements characterizing the light scattering and absorption properties of seawater. Previous studies have demonstrated relationships between these optical properties of seawater and various metrics of particle size, including specific percentile diameters such as $D_V(50)$ and $D_V(90)$ (Koestner et al., 2020; Woźniak et al., 2010). The results of this study suggest that alternative percentile diameters obtained from the cumulative distribution functions of particle number, area, and volume concentration, chosen to target specific size class partitions based on the pico-, nano-, and microplankton classes, provide a powerful new approach to characterize the complex shape of the PSD. It is notable that this approach can also be extended to a broader size range than encompassed by this study if adequate PSD measurements become available, and also appears adaptable to targeting the estimation of other size intervals as required by a given scientific problem. It is also likely that the basic conceptual approach is suitable for use with other natural particle assemblages, such as those found in sedimentary layers or in the atmosphere. These extensions would naturally require additional work and analyses to determine the appropriate percentile diameters. Perhaps most importantly, the proposed approach offers promising prospects to greatly extend the spatial and temporal observation capabilities of the PSD for both regional and global studies of particle dynamics in the oceanic environment if adequate quantitative relationships can be established between optical measurements of seawater and the percentile diameters that serve as reliable predictors of individual particle size class contributions. Further research is thus needed to explore such relationships between these percentile diameters and suitable optical proxies that are amenable to measurement from optical sensors mounted on either autonomous underwater vehicles or above water platforms such as aircraft or satellites.

Conflict of Interest

The authors declare that the research was conducted in the absence of any commercial or financial relationships that could be construed as a potential conflict of interest.

Data Availability Statement

The final particle size distribution measurements used in this study are publicly available on the Dryad Digital Repository (https://doi.org/10.6076/D16C77). Original measurements and ancillary data for most of the cruises utilized in this study are also publicly available in the following online repositories: LEFE-CYBER database (http://www.obs-vlfr.fr/proof/index_vt.htm; BIOSOPE), SEA scieNtific Open data Edition (https://www.seanoe.org/data/00641/75345/; MALINA), the NASA SeaWiFS Bio-optical Archive and Storage System (https://seabass.gsfc.nasa.gov/; HLY1001, HLY1101), and the Data and Sample Research System for Whole Cruise Information database of the Japan Agency for Marine-Earth Sciences (https://doi.org/10.17596/0001879; MR1705-C cruise).

References

Agrawal, Y. C., & Pottsmith, H. C. (2000). Instruments for particle size and settling velocity observations in sediment transport. *Marine Geology*, *168*, 89–114. https://doi.org/10.1016/s0025-3227(00)00044-x

Bader, H. (1970). The hyperbolic distribution of particle sizes. *Journal of Geophysical Research*, *75*, 2822–2830. https://doi.org/10.1029/JC075i015p02822

Baker, E. T., & Lavelle, J. W. (1984). The effect of particle size on the light attenuation coefficient of natural suspensions. *Journal of Geophysical Research*, *89*, 8197–8203. https://doi.org/10.1029/jc089ic05p08197

Barndorff-Nielsen, O. (1977). Exponentially decreasing distributions for the logarithm of particle size. *Proceedings of the Royal Society of London*, *353*, 401–419.

Beaton, A. E., & Tukey, J. W. (1974). The fitting of power series, meaning polynomials, illustrated on band-spectroscopic data. *Technometrics*, *16*, 147–185. https://doi.org/10.1080/00401706.1974.10489171

Bernard, S., Shillington, F. A., & Probyn, T. A. (2007). The use of equivalent size distributions of natural phytoplankton assemblages for optical modeling. *Optics Express*, *15*, 1995–2007. https://doi.org/10.1364/oe.15.001995

Bochdansky, A. B., Clouse, M. A., & Herndl, G. J. (2016). Dragon kings of the deep sea: Marine particles deviate markedly from the common number-size spectrum. *Scientific Reports*, *6*, 22633. https://doi.org/10.1038/srep22633

Bowers, D. G., Binding, C. E., & Ellis, K. M. (2007). Satellite remote sensing of the geographical distribution of suspended particle size in an energetic shelf sea. *Estuarine, Coastal and Shelf Science*, *73*, 457–466. https://doi.org/10.1016/j.ecss.2007.02.005

Briggs, N. T., Slade, W. H., Boss, E., & Perry, M. J. (2013). Method for estimating mean particle size from high frequency fluctuations in beam attenuation or scattering measurements. *Applied Optics*, *52*, 6710–6725. https://doi.org/10.1364/AO.52.006710

Brun-Cottan, J. C. (1971). Etude de la granulométrie des particules marines, mesures effectuées avec un compteur Coulter. *Cahiers Oceano-graphiques*, *23*, 193–205.

Buonassissi, C. J., & Dierssen, H. M. (2010). A regional comparison of particle size distributions and the power law approximation in oceanic and estuarine surface waters. *Journal of Geophysical Research*, *115*, C10028. https://doi.org/10.1029/2010JC006256

Burd, A. B. (2013). Modeling particle aggregation using size class and size spectrum approaches. *Journal of Geophysical Research*, *118*, 3431–3443. https://doi.org/10.1002/jgrc.20255

Carder, K. L., Beardsley, G. F., Jr, & Pak, H. (1971). Particle size distributions in the eastern equatorial Pacific. *Journal of Geophysical Research*, *76*, 5070–5077. https://doi.org/10.1029/jc076i021p05070

Ceronio, A. D., & Haarhoff, J. (2005). An improvement on the power law for the description of particle size distributions in potable water treatment. *Water Research*, *39*, 305–313. https://doi.org/10.1016/j.watres.2004.09.023

Chisholm, S. W. (1992). Phytoplankton size. In P. G. Falkowski, & A. D. Woodhead (Eds.), *Primary productivity and biogeochemical cycles in the sea* (pp. 213–237). Plenum Press. https://doi.org/10.1007/978-1-4899-0762-2_12

Claustre, H., Sciandra, A., & Vaulot, D. (2008). Introduction to the special section bio-optical and biogeochemical conditions in the South East Pacific in late 2004: the BIOSOPE program. *Biogeosciences*, *5*, 679–691. https://doi.org/10.5194/bg-5-679-2008

Dickey, T., Banner, M., Bhandari, P., Boyd, T., Carvalho, L., Chang, G., et al. (2012). Introduction to special section on recent advances in the study of optical variability in the near-surface and Upper Ocean. *Journal of Geophysical Research*, *117*, C00H20. https://doi.org/10.1029/2012JC007964

Gordon, H. R., & Brown, O. B. (1972). A theoretical model of light scattering by Sargasso Sea particulates. *Limnology & Oceanography*, *17*, 826–832. https://doi.org/10.4319/lo.1972.17.6.0826

Graham, G. W., & Nimmo-Smith, W. A. (2010). The application of holography to the analysis of size and settling velocity of suspended cohesive sediments. *Limnology and Oceanography: Methods*, *8*, 1–15. https://doi.org/10.4319/lom.2010.8.1

IOCCG. (2014). Phytoplankton functional types from space. In S. Sathyendranath (Ed.), *Reports of the International Ocean Colour Coordinating Group* (Vol. 15). International Ocean Colour Coordinating Group. https://doi.org/10.1111/imre.12086

Jackson, G. A. (1995). Comparing observed changes in particle size spectra with those predicted using coagulation theory. *Deep-Sea Research Part II*, *42*, 159–184. https://doi.org/10.1016/0967-0645(95)00010-n

Jackson, G. A., Maffione, R., Costello, D. K., Alldredge, A. L., Logan, B. E., & Dam, H. G. (1997). Particle size spectra between 1 μm and 1 cm at Monterey Bay determined using multiple instruments. *Deep-Sea Research Part I*, *44*, 1739–1767. https://doi.org/10.1016/s0967-0637(97)00029-0

Jennings, S., & Warr, K. J. (2003). Smaller predator-prey body size ratios in longer food chains. *Proceedings of the Royal Society of London B Biological Sciences*, *270*, 1413–1417. https://doi.org/10.1098/rspb.2003.2392

Johnsen, S., Gassman, E., Reynolds, R. A., Stramski, D., & Mobley, C. (2014). The asymmetry of the underwater light field and its implications for mirror-based camouflage in silvery pelagic fish. *Limnology & Oceanography*, *59*, 1839–1852. https://doi.org/10.4319/lo.2014.59.6.1839

Jonasz, M. (1983). Particle-size distributions in the Baltic. *Tellus B: Chemical and Physical Meteorology*, *35*, 346–358. https://doi.org/10.3402/tellusb.v35i5.14624

Jonasz, M., & Fournier, G. (1996). Approximation of the size distribution of marine particles by a sum of log-normal functions. *Limnology & Oceanography*, *41*, 744–754. https://doi.org/10.4319/lo.1996.41.4.0744

Jonasz, M., & Fournier, G. (2007). *Light scattering by particles in water: Theoretical and experimental foundations*: Academic Press.

Junge, C. E. (1963). *Air Chemistry and radioactivity*. Academic Press.

Kiefer, D. A., & Berwald, J. (1992). A random encounter model for the microbial planktonic community. *Limnology & Oceanography*, *37*, 457–467. https://doi.org/10.4319/lo.1992.37.3.0457

Kitchen, J. C., Menzies, D., Pak, H., Zaneveld, J. R. V., & Zaneveld, V. (1975). Particle size distributions in a region of coastal upwelling analyzed by characteristic vectors. *Limnology & Oceanography*, *20*, 775–783. https://doi.org/10.4319/lo.1975.20.5.0775

Koestner, D., Stramski, D., & Reynolds, R. A. (2020). Assessing the effects of particle size and composition on light scattering through measurements of size-fractionated seawater samples. *Limnology & Oceanography*, *65*, 173–190. https://doi.org/10.1002/lno.11259

Koike, I., Hara, S., Terauchi, K., & Kogure, K. (1990). Role of sub-micrometre particles in the ocean. *Nature*, *345*, 242–244. https://doi.org/10.1038/345556a0

Kostadinov, T. S., Siegel, D. A., & Maritorena, S. (2009). Retrieval of the particle size distribution from satellite ocean color observations. *Journal of Geophysical Research*, *114*, C09015. https://doi.org/10.1029/2009JC005303

Kostadinov, T. S., Siegel, D. A., & Maritorena, S. (2010). Global variability of phytoplankton functional types from space: Assessment via the particle size distribution. *Biogeosciences*, *7*, 3239–3257. https://doi.org/10.5194/bg-7-3239-2010

Kranck, K., & Milligan, T. G. (1992). Characteristics of suspended particles at an 11-hour anchor station in San Francisco Bay, California. *Journal of Geophysical Research*, *97*, 11373–11382. https://doi.org/10.1029/92jc00950

Lambert, C. E., Jehanno, C., Silverberg, N., Brun-Cottan, J. C., & Chesselet, R. (1981). Log-normal distributions of suspended particles in the open ocean. *Journal of Marine Research*, *30*, 77–98. https://doi.org/10.2307/2346663

Lawler, D. F. (1997). Particle size distributions in treatment processes: Theory and practice. *Water Science and Technology*, *36*, 15–23. https://doi.org/10.2166/wst.1997.0075

Le Quéré, C. L., Harrison, S. P., Colin Prentice, I., Buitenhuis, E. T., Aumont, O., Bopp, L., et al. (2005). Ecosystem dynamics based on plankton functional types for global ocean biogeochemistry models. *Global Change Biology*, *11*, 2016–2040. https://doi.org/10.1111/j.1365-2486.2005.1004.x

Lei, S., Xu, J., Li, Y., Li, L., Lyu, H., Liu, G., et al. (2021). A semi-analytical algorithm for deriving the particle size distribution slope of turbid inland water based on OLCI data: A case study in Lake Hongze. *Environmental Pollution*, *270*, 116288. https://doi.org/10.1016/j.envpol.2020.116288

Marañón, E. (2015). Cell size as a key determinant of phytoplankton metabolism and community structure. *Annual Review of Marine Science*, *7*, 241–264. https://doi.org/10.1146/annurev-marine-010814-015955

McCave, I. N. (1984). Size spectra and aggregation of suspended particles in the deep ocean. *Deep-Sea Research*, *31*, 329–352. https://doi.org/10.1016/0198-0149(84)90088-8

Mikkelsen, O. A., Hill, P. S., & Milligan, T. G. (2006). Single-grain, microfloc and macrofloc volume variations observed with a LISST-100 and a digital floc camera. *Journal of Sea Research*, *55*, 87–102. https://doi.org/10.1016/j.seares.2005.09.003

Moore, C., Barnard, A., Fietzek, P., Lewis, M. R., Sosik, H. M., White, S., et al. (2009). Optical tools for ocean monitoring and research. *Ocean Science*, *5*, 661–684. https://doi.org/10.5194/os-5-661-2009

Moré, J. J. (1978). The Levenberg-Marquardt algorithm: Implementation and theory. In G. A. Watson (Ed.), *Numerical analysis* (pp. 105–116). Springer. https://doi.org/10.1007/bfb0067700

Morel, A., & Bricaud, A. (1986). Inherent optical properties of algal cells including picoplankton: Theoretical and experimental results. *Canadian Bulletin of Fisheries and Aquatic Sciences*, *214*, 521–559.

Organelli, E., Dall'Olmo, G., Brewin, R. J. W., Nencioli, F., & Tarran, G. A. (2020). Drivers of spectral optical scattering by particles in the upper 500 m of the Atlantic Ocean. *Optics Express*, *28*, 34147–34166. https://doi.org/10.1364/OE.408439

Organelli, E., Dall'Olmo, G., Brewin, R. J. W., Tarran, G. A., Boss, E., & Bricaud, A. (2018). The open-ocean missing backscattering is in the structural complexity of particles. *Nature Communications*, *9*, 5439. https://doi.org/10.1038/s41467-018-07814-6

Parsons, T. R. (1969). The use of particle size spectra in determining the structure of a plankton community. *Journal of the Oceanographical Society of Japan*, *25*, 172–181. https://doi.org/10.5928/kaiyou1942.25.172

Picheral, M., Guidi, L., Stemmann, L., Karl, D. M., Iddaoud, G., & Gorsky, G. (2010). The Underwater Vision Profiler 5: An advanced instrument for high spatial resolution studies of particle size spectra and zooplankton. *Limnology and Oceanography: Methods*, *8*, 462–473. https://doi.org/10.4319/lom.2010.8.462

Platt, T., & Denman, K. L. (1978). The structure of pelagic marine ecosystems. *Rapports et Proces-Verbaux des Reunions Consell International pour I'Exploration de la Mer*, *173*, 60–65.

Qiu, Z., Sun, D., Hu, C., Wang, S., Zheng, L., Huan, Y., et al. (2016). Variability of particle size distributions in the Bohai Sea and the Yellow Sea. *Remote Sensing*, *8*, 949. https://doi.org/10.3390/rs8110949

Reynolds, R. A., & Stramski, D. (2021). *Oceanic particle size distributions for the PacAtl and Arctic datasets*. Dryad. https://doi.org/10.6076/D16C77

Reynolds, R. A., Stramski, D., & Neukermans, G. (2016). Optical backscattering of particles in Arctic seawater and relationships to particle mass concentration, size distribution, and bulk composition. *Limnology & Oceanography*, *61*, 1869–1890. https://doi.org/10.1002/lno.10341

Reynolds, R. A., Stramski, D., Wright, V. M., & Woźniak, S. B. (2010). Measurements and characterization of particle size distributions in coastal waters. *Journal of Geophysical Research*, *115*, C08024. https://doi.org/10.1029/2009JC005930

Rinaldo, A., Maritan, A., Cavender-Bares, K. K., & Chisholm, S. W. (2002). Cross-scale ecological dynamics and microbial size spectra in marine ecosystems. *Proceedings of Royal Society Biological Science*, *269*, 2051–2059. https://doi.org/10.1098/rspb.2002.2102

Risović, D. (1993). Two-component model of sea particle size distribution. *Deep-Sea Research Part I*, *40*, 1459–1473. https://doi.org/10.1016/0967-0637(93)90123-K

Runyan, H., Reynolds, R. A., & Stramski, D. (2020). Evaluation of particle size distribution metrics to estimate the relative contributions of different size fractions based on measurements in Arctic waters. *Journal of Geophysical Research Science: Oceans*, *125*, e2020JC016218. https://doi.org/10.1029/2020JC016218

Sheldon, R. W., Prakash, A., & Sutcliffe, W. H., Jr. (1972). The size distribution of particles in the ocean. *Limnology & Oceanography*, *17*, 327–340. https://doi.org/10.4319/lo.1972.17.3.0327

Sheldon, R. W., Sutcliffe, W. H., Jr, & Paranjpe, M. A. (1977). Structure of planktonic food chains and relationship between plankton and fish production. *Journal of the Fisheries Research Board of Canada*, *34*, 2344–2353. https://doi.org/10.1139/f77-314

Shi, W., & Wang, M. (2019). Characterization of suspended particle size distribution in global highly turbid waters from VIIRS measurements. *Journal of Geophysical Research*, *124*, 3796–3817. https://doi.org/10.1029/2018JC014793

Sieburth, J. M., Smetacek, V., & Lenz, J. (1978). Pelagic ecosystem structure: Heterotrophic compartments of the plankton and their relationship to plankton size fractions. *Limnology & Oceanography*, *23*, 1256–1263. https://doi.org/10.4319/lo.1978.23.6.1256

Slade, W. H., & Boss, E. (2015). Spectral attenuation and backscattering as indicators of average particle size. *Applied Optics*, *54*, 7264–7277. https://doi.org/10.1364/AO.54.007264

Stavn, R. H. (2004). Suspended minerogenic particle distributions in high-energy coastal environments: Optical implications. *Journal of Geophysical Research*, *109*, 201–219. https://doi.org/10.1029/2003JC002098

Stemmann, L., & Boss, E. (2012). Plankton and particle size and packaging: From determining optical properties to driving the biological pump. *Annual Review of Marine Science*, *4*, 263–290. https://doi.org/10.1146/annurev-marine-120710-100853

Stemmann, L., Eloire, D., Sciandra, A., Jackson, G. A., Guidi, L., Picheral, M., et al. (2008). Volume distribution for particles between 3.5 to 2000 μm in the upper 200 m region of the South Pacific Gyre. *Biogeosciences*, *5*, 299–310. https://doi.org/10.5194/bg-5-299-2008

Stemmann, L., Jackson, G. A., & Ianson, D. (2004). A vertical model of particle size distributions and fluxes in the midwater column that includes biological and physical processes — Part I model formulation. *Deep-Sea Research Part I*, *51*, 865–884. https://doi.org/10.1016/j.dsr.2004.03.001

Stramski, D., & Kiefer, D. A. (1991). Light scattering by microorganisms in the open ocean. *Progress in Oceanography*, *28*, 343–383. https://doi.org/10.1016/0079-6611(91)90032-h

Stramski, D., Reynolds, R. A., Gernez, P., Röttgers, R., & Wurl, O. (2019). Inherent optical properties and particle characteristics of the sea-surface microlayer. *Progress in Oceanography*, *176*, 102117. https://doi.org/10.1016/j.pocean.2019.05.009

Uitz, J., Stramski, D., Reynolds, R. A., & Dubranna, J. (2015). Assessing phytoplankton community composition from hyperspectral measurements of phytoplankton absorption coefficient and remote-sensing reflectance in open-ocean environments. *Remote Sensing of Environment*, *171*, 58–74. https://doi.org/10.1016/j.rse.2015.09.027

Ward, B. A., Dutkiewicz, S., Jahn, O., & Follows, M. J. (2012). A size-structured food-web model for the global ocean. *Limnology & Oceanography*, *57*, 1877–1891. https://doi.org/10.4319/lo.2012.57.6.1877

Wells, M. L., & Goldberg, E. D. (1991). Occurrence of small colloids in sea water. *Nature*, *353*, 342–344. https://doi.org/10.1038/353342a0

Woźniak, S. B., Stramski, D., Stramska, M., Reynolds, R. A., Wright, V. M., Miksic, E. Y., et al. (2010). Optical variability of seawater in relation to particle concentration, composition, and size distribution in the nearshore marine environment at Imperial Beach, California. *Journal of Geophysical Research*, *115*, C08027. https://doi.org/10.1029/2009JC005554

Xi, H., Larouche, P., Tang, S., & Michel, C. (2014). Characterization and variability of particle size distributions in Hudson Bay, Canada. *J. Geophys. Res. Oceans*, *119*, 3392–3406. https://doi.org/10.1002/2013JC009542

Zhang, X., Twardowski, M., & Lewis, M. (2012). Retrieving composition and sizes of oceanic particle subpopulations from the volume scattering function. *Applied Optics*, *50*, 1240–1259.